Journal of Trace Elements in Medicine and Biology 52 (2019) 270–287

Contents lists available at ScienceDirect

Journal of Trace Elements in Medicine and Biology

journal homepage: www.elsevier.com/locate/jtemb

Toxicology

Sub-acute oral exposure of zinc oxide nanoparticles causes alteration in iron homeostasis through acute phase response: A protective effect by surface modification

Anurag Kumar Srivastav[a,b], Nitesh Dhiman[c,d], Ratnakar Tiwari[e], Nidhi Arjaria[f], Jyoti Prakash[b], Pankaj Jagdale[g], Anjaneya Ayanur[g], Dhirendra Singh[g], Satyakam Patnaik[c,d], Mahadeo Kumar[a,*]

[a] Biochemistry Laboratory, Animal Facility, Regulatory Toxicology Group, CSIR-Indian Institute of Toxicology Research (CSIR-IITR), Vishvigyan Bhavan, 31, Mahatma Gandhi Marg, Lucknow 226001, Uttar Pradesh, India
[b] Amity Institute of Biotechnology, Amity University Uttar Pradesh, Lucknow Campus, Lucknow 226028, Uttar Pradesh, India
[c] Water Analysis Laboratory, Nanotherapeutics and Nanomaterials Toxicology Group, CSIR-Indian Institute of Toxicology Research, (CSIR-IITR), Vishvigyan Bhavan, 31, Mahatma Gandhi Marg, Lucknow 226001, Uttar Pradesh, India
[d] Academy of Scientific and Innovative Research (AcSIR), CSIR-Indian Institute of Toxicology Research (CSIR-IITR), Lucknow 226001, Uttar Pradesh, India
[e] Developmental Toxicology Laboratory, Systems Toxicology and Health Risk Assessment Group, CSIR-Indian Institute of Toxicology Research, Vishvigyan Bhavan, Lucknow 226001, Uttar Pradesh, India
[f] Advanced Imaging Facility, CSIR-Indian Institute of Toxicology Research, Vishvigyan Bhavan, Lucknow, India
[g] Central Pathology Laboratory, Regulatory Toxicology Group, CSIR-Indian Institute of Toxicology Research (CSIR-IITR), Vishvigyan Bhavan, 31, Mahatma Gandhi Marg, Lucknow 226001, Uttar Pradesh, India

ARTICLE INFO

Keywords:
ZnO
Nanoparticles
Inflammation
Sub-acute
Anemia
Acute phase

ABSTRACT

Zinc oxide nanoparticles (ZnO NPs) are one of the most widely used nanomaterials. Following oral exposure, these NPs can accumulate in various organs and induce the toxicity due to their physiochemical characteristics. In present study to reduce the toxicity, surface engineered ZnO NPs (c-ZnO NPs) were *in-situ* synthesized by using polyacrylamide grafted guar gum (PAm-g-GG) polymer in alkaline media. Further, the comparative effect of bared ZnO NPs (b-ZnO NPs) and c-ZnO NPs were assessed on secondary target organ liver and kidneys of Swiss mice at doses of 10, 50 and 300 mg/kg following 28 days repeated oral treatment. The b-ZnO NPs were incited severe damages in liver and kidney tissue than c-ZnO NPs as seen by transmission electron microscopy and histopathology. The increased levels of serum biomarkers (AST, ALT, ALP, creatinine, uric acid, and urea) were also observed, that remarking a disturbance in the function of liver and kidney. After sub-acute oral treatment of b-ZnO NPs, the hepatic pro-inflammatory cytokines (IL-6, TNF-α, and MMP-9) were up-regulated that causes the activation of acute phase response (APR). We also observed significantly increased in expression of hepatic acute phase proteins (hepcidin and haptoglobin) and altered interlinked iron (Fe) signaling biomarkers (hephaestin, TF, TFR-1, LDH, and ferroportin). This study emphasizes that exposure to ZnO NPs may cause inflammation mediated APR through ultra-structural damage of tissue that could escort the progression of anemia. Nevertheless, the capping with PAm-g-GG in c- ZnO NPs has reduced the toxicity by altering the surface reactive property of ZnO NPs.

1. Introduction

Nanoscale semiconductors have gained much attention in current era owing to their unique electronic, optical, structural and thermal properties which are believed to offer extraordinary economic and societal benefits [1]. A report given by Sargent has addressed the online inventory of consumer products having a number of 1682 engineered nanoparticles (NPs) [2], and the global nanotechnology market expected to reach $90.5 billion by 2021 from $39.2 billion in 2016 at a compound annual growth rate of 18.2% [3]. Among these, zinc oxide (ZnO) NPs have been widely applicable in therapeutics, sunscreens, biosensors, food additives, catalyst, pigments and electronic materials due to their chemical stability, strong adsorption ability and antibacterial activity [4,5]. These NPs are shown to be superior in the selective destruction of tumor cells and suitable tool in drug delivery and sensing horizon [6]. Thus, the progressive use of ZnO NPs has increased

* Corresponding author.
E-mail address: mahadeo@iitr.res.in (M. Kumar).

https://doi.org/10.1016/j.jtemb.2019.01.008
Received 17 August 2018; Received in revised form 4 December 2018; Accepted 13 January 2019

the concerns with regards to toxicity because the possibility of the exposure of these NPs into the body is rising by the direct or indirect way including ingestion, inhalation and dermal. Along with oral route, Inhalation is also a common exposure route of the working environment but a part of the inhaled particles are removed from the lungs by the mucociliary defense system and then swallowed entering gastrointestinal tract. Thus, intake of NPs via gastrointestinal tract is one of the prime routes [7,8]. In biological fluid, the novel properties of NPs are related to their size, shape, and surface chemistry. The nano-sized particles have the high specific surface area to mass ratio, that promotes their accumulation along with increased reactivity with biomolecules after entered in the biological system [9]. Hitherto, few researchers have been investigated the ZnO NPs induced organ-specific toxicity based on surface characteristics, size, dissolution, exposure routes and structures of NPs [7,9–11], but their mechanistic role in Fe signaling pathway is still not well explained. The repeated dose of ZnO NPs enhances the zinc (Zn) level in the body that may slow down the absorption of copper (Cu) and iron (Fe) [12,13]. Willis et al., had been reported the antagonistic effect on Cu absorption with Zn [12]. This decreased level of Cu may suppress the Cu activated metallotransferase activity such as ferroxidase that plays a vital role in Fe absorption [12]. Lloblet et al., has been studied the chronic exposure (90 days) of Zn suspension (640 mg/kg body weight) that consequently decreased the Fe level [14]. Clancey and Murphy were reported that higher Zn exposure is responsible for induced hemolytic anemia in the dog [15]. These divalent cations Fe and Zn share the same enterocyte transporter, that shows a potential opposite interaction between these two micro-minerals [16]. Furthermore, many prior works have only substantiated the ZnO NPs induced acute phase response (APR) that resultant in an inflated expression of inflammatory biomarkers in the secondary target organ. It was properly known that the conjunction of APR alter the interlinked signaling pathway for Fe homeostasis, such as: transferrin receptor 1 (TFR-1), hephaestin (Heph), ferroportin (FPN), hepcidin (Hep), transferrin (TF), haptoglobin (Hp) and pro-inflammatory biomarkers (matrix metalloproteinase-9 (MMP-9), tissue inhibitor of metalloproteinase-2 (TIMP-2), Interleukin-6 (IL-6) and tissue necrotic factor-α (TNF-α). Thus, concerning the above findings, in the present study we evaluated the effect of ZnO NPs on Fe homeostasis.

Here, we hypothesized that the ZnO NPs induced APR might be altered the signaling pathway of Fe homeostasis that decreases the level of iron in circulation. Additionally, the long-term exposure of ZnO NPs might be upshot the hemolytic anemia progression by lowering the RBC formation through depletion of iron or bruised the RBCs membrane due to direct binding, or induction of reactive oxygen species (ROS). In this context, we opted surface modified ZnO NPs to reduce the toxicity and compared with bare NPs to attract a great deal of attention in Fe homeostasis. For surface modification, the ZnO NPs were synthesized by using hydrophilic non-ionic polyacrylamide (PAm) grafted guar gum (GG) (PAm-g-GG) capped ZnO NPs (c-ZnO NPs). GG is a bio-safe and compatible galactomannan polysaccharides and pertains to colon-specific drug delivery system, hypoglycemia and oral drug delivery [17].

The *in vivo* 28 days oral toxicity study of c-ZnO NPs with the comparison to bared ZnO (b-ZnO) NPs at three defined doses 10, 50 and 300 mg/kg were carried out to assess the toxicity on secondary targeted organ (liver and kidney) and analyze the expected interlinked Fe homeostatic biomarkers TFR-1, TFR-2, Heph, hepcidin, transferrin, ferroportin, Hp and inflammatory biomarkers at gene and protein level. The doses were decided based on previously reported low observe adverse effect level (LOAEL) for oral exposure experiments [18]. The highest dose was selected based on the induction of a toxic effect without severe sufferings and mortality, whereas the lowest dose demonstrated slight adverse effects.

2. Materials and methods

2.1. Chemicals and reagents

The bared ZnO NPs (b-ZnO NPs; < 50 nm), GG, zinc acetate dihydrate, acrylamide, protease, and phosphatase inhibitors, fluoroshield 4',6 diamidino-2-phenylindole (DAPI), DNAse1 and hot start polymerase chain reaction (PCR) master mix were obtained from Sigma-Aldrich, USA. Commercial GG was cleansed by using methanol. Trizol reagent, 2, 7-dichlorofluorescein diacetate (DCF-DA) reagent, rhodamine phalloidin and high capacity cDNA reverse transcription kit was purchased from Thermo Fisher Scientific, USA. Primers for real-time (RT) PCR were received from Integrated DNA technologies (IDT), USA. The haptoglobin (Hp), matrix metalloproteinase-9 (MMP-9) and tissue inhibitor of metalloproteinase-2 (TIMP-2) antibodies were procured from Zymo Research Corporation, USA. β-actin antibody was received from Abcam, USA. All other chemicals used in the study were of analytical grade.

2.2. Synthesis of PAm-g-GG capped ZnO (c-ZnO) NPs

The engrafting of PAm on GG has been adopted according to the previous report to enhance shelf life and to provide spacer onto GG [19]. Concisely, methanol purified GG 300 mg and 0.014 mol (995.26 mg) acrylamide monomer were dissolved in 75 mL Milli-Q at 27 °C. Afterward, redox initiators; permanganate (0.0015 mol) and oxalic acid (0.0037 mol) were added and allowed to raise temperature of reaction mixture at 37 °C for 2 h with perpetual stirring in an inert environment. After concluding the reaction, the mixture was poured in methanol: water (35:15 v/v) to removed PAm homopolymer and lyophilized for further use.

To achieve less viscous ≤ 50 nm ZnO NPs solution for effective oral delivery, some modification has been made in synthesis protocol [20]. Briefly, zinc acetate dihydrate (5 mmol) was dissolved in 2-propanol (100 mL) with vigorous stirring at 50 °C. Subsequently, synthesized PAm-g-GG polymer (30 mg) was dispersed in Milli-Q (1150 mL) and mixed to above anhydrous Zn $(CH_3COO)_2$ solutions. Finally, 1 N NaOH (prepared in 2-propanol) was added into obtained homogeneous solution with dynamic stirring for 2 h at 0 °C. The precipitate was collected using a centrifugation at 4000*g* for 10 min and lyophilized for further use.

2.3. Characterizations of NPs

Modified functional group analysis of GG and synthesized c-ZnO NPs were performed with attenuated total reflectance-fourier transform infrared (ATR-FTIR) spectra (Thermo Fischer: Nicolet, iS5, USA) in comparison to b-ZnO NPs. The absorbance spectra of c-ZnO and b-ZnO NPs were collected by UV–vis double beam spectrophotometer (Perkin Elmer, Lambda 35, USA). Quantification of Zn in c-ZnO NPs was performed by using atomic absorption spectroscopy (AAS, Avanta-R; GBC, VIC, Australia) at 213.9 nm after digestion with HNO_3: $HClO_4$ (6:1) to leaching out Zn metal. The hydrodynamic diameter and zeta potential of c-ZnO and b-ZnO NPs in solutions were measured by Dynamic light scattering (DLS) using a zetasizer (Nano-ZSP Malvern, UK) equipped with a green laser (523 nm). The intensity of the back-scattered light was detected at the angle of 173°. The transmission electron microscope (TEM) (FEI Technai G-2 spirit, Netherland) operated at 80 kV with 15,000× magnifications to determine actual size and shape of c-ZnO and b-ZnO NPs.

For stability and release assessment of soluble Zn from ZnO NPs, 5 mL of freshly prepared doses (medium is Milli-Q, Ph-7.2) were kept at room temperature for 24 h. They were then ultra-centrifuged at 100,000*g* for one hour to settle ZnO NPs. After centrifugation, the supernatant and precipitate was separated and analyzed with atomic absorption spectrophotometer (AAS) to check the amount of Zn^{2+} and

total ZnO NPs.

2.4. Preparation of simulated and mouse extracted gastric fluid

The simulated gastric fluid was prepared by dissolving 2 g sodium chloride and 3.2 g pepsin in Milli-Q, and the pH was adjusted to 1.5 with 1 N hydrochloric acid and then made up to 1000 mL. The mouse gastric fluid was obtained as previously reported [21]. Briefly, stomach was collected and rinsed with saline, and then gastric fluids were obtained by centrifugation at 16,000*g* for 15 min at 4 °C.

2.5. Dissolution properties of ZnO NPs in biological fluids

The bared and capped ZnO NPs suspension were added to simulated and mouse-extracted biofluid (gastric fluid and serum) (5 mg/mL) and incubated at 37 °C for 1 h with constant shaking (180 rpm). After incubation centrifuged the sample at 15,000*g* for 15 min and the supernatants were collected for estimation of dissolve Zn through AAS. The characterization of NPs in biofluid was performed based on previous literature [21,22]. For pre-digestion of collected supernatant, added 10 mL of 60% ultrapure nitric acid and 0.5 mL of H_2O_2 at 180 °C. The digested solutions were diluted with 2.5 mL of Milli-Q and quantitative analysis of the dissolved Zn from ZnO was carried out using AAS (Avanta-R; GBC, VIC, Australia).

2.6. Animals and their housing

Adult female Swiss mice aged 5 weeks, weight 25–30 g were received with the consent of institutional animal ethics committee (Approval No.CSIR/IITR/IAEC/48/2016) from the animal facility of CSIR-Indian Institute of Toxicology Research, Lucknow, India and were acclimatized for 5 days before start the experiment. The experimental animals were housed in standard environmental conditions (12 h light/dark cycle at 22 ± 2 °C and relative humidity 50 ± 10%). The mice were fed with specified pellet diet *ad libitum* and free access to water.

The mice were randomly divided into 7 groups (G1 to G7) containing 10 animals in each group; Group 1 (G1) control mice, treated with Milli-Q water, group 4, 3, and 2 (G4, G3, and G2) were treated with b-ZnO NPs at the dose of 10 mg/kg, 50 mg/kg and 300 mg/kg body weight, similarly group 7, 6, and 5 (G7, G6, and G5) were treated with same dose of c-ZnO NPs, respectively. The dosages were administered by oral gavages, once daily for 28 days under normal feeding condition. These dose formulations were decided based on previously reported LOAEL for oral exposure study conducted following OECD guidelines [7,18]. Before each dosing, the NPs suspensions were ultra-sonicated for 10 min at 45 s sonic on/15 s off condition (Sonics, Vibracell, USA). The suspensions were administered at a dose volume of 1 mL/100 g body weight. The body weights growth rate and food consumption of all animals were recorded weekly during the experimental period. After 28 days of post-treatment, all animals of each group were sacrificed for the assessment of toxicity associated with Fe homeostasis.

2.7. Samples collection for various assay

The blood samples were collected from all animals of each group at the time of necropsy for hematological, AAS and biochemical analysis. The animals were anesthetized with ketamine and blood samples were taken via cardiac puncture and transferred it into K_2-EDTA coated vacutainer for hematology and in plain vacutainer for biochemical analysis. Liver, kidney, and intestine were isolated for further assays.

The collected liver and kidney tissues from 5 animals of each group were perfused with 100 mL of ice-cold saline (0.9% NaCl in deionized) and fixed in 4% paraformaldehyde (PFA) for histopathology, immunohistochemistry and TEM analysis. Additionally, the intestine was taken for immunohistochemistry (IHC). Remaining tissue of 5 animals was snap frozen in liquid nitrogen and kept at -80 °C for real-time (RT) PCR, ROS, and western blotting.

2.8. Determination of Zn accumulation in liver, kidney, and plasma

The collected plasma (0.2 mL), liver and kidney tissue (0.2 g) from each group's animal (as described in Section 2.7) were digested with HNO_3 and $HClO_4$ (6:1) at 190 °C, then the sample volume was makeup to 10 mL with acidic water (1 N HNO_3). The determination of Zn content was performed by AAS (Avanta-R; GBC, VIC, Australia).

2.9. Detection of ZnO NPs and Zn^{2+} ratios in tissue

Accumulation of Zn solute and NP matrix ratio in liver and kidney were measured as recently assessed by Tiwari et al., [23]. Triton X-114 (TX-114)-based cloud point extraction (CPE) was used to differentiate the amount of ZnO NPs and Zn^{2+} in the tissue [24]. For this assay, an equal amount of tissue (wet weight) was homogenized in double distilled water (DDW) and the volume adjusted to 10 mL with DDW. The pH was adjusted to 3.5 with 10% HNO_3 to achieve better phase separation. After adjusting pH, 200 µL of 1 M $Na_2S_2O_3$ and 10% (w/v) triton X-114 was added and mixed properly. The mixture was incubated for 1 h at 40 °C and then centrifuged at 5000*g* for 15 min. The supernatant was carefully separated and further incubated for 30 min at 40 °C. Further centrifuged at 5000*g*, the supernatant and precipitate were separated. The precipitates and collected supernatants were processed for AAS to check concentration in the supernatant (Zn^{2+}) and precipitate (nonionic, ZnO NPs).

2.10. Cellular internalization of NPs by TEM analysis

In order to assess the cellular uptake of NPs with respect to surface functionality and charges, TEM analysis of liver and kidney tissues have been performed in the high dose of b-ZnO and c-ZnO NPs (G2 and G5 group) with respect to control (G1) after 28 days repeated oral treatment. In this context, the perfused liver and kidney tissue samples were fixed in 4% paraformaldehyde containing 0.5% glutaraldehyde prepared in 0.1 M cacodylate buffer (Ladd Research Industries, USA) at 4 °C for 2 h.

Tissues were washed thrice in 0.1 M sodium cacodylate buffer and post-fixed in 1% osmium tetraoxide prepared in 0.2 M cacodylate buffer for 2 h. The fixed tissues were again washed three times with 0.1 M sodium cacodylate buffer, dehydrated in acetone gradient (15–100%), and embedded in araldite-DDSA mixture (Ladd Research Industries, USA). After baking at 60 °C, blocks were cut (60–80 nm thick) by ultramicrotome (Leica EM UC7) and sections were analyzed under FEI Technai G2 spirit twin TEM equipped with gatan digital CCD Camera (Netherland) at 60 or 80 KV.

2.11. Histopathological analysis

Histopathological analysis was performed for evaluating pathological lesions in liver and kidneys. The tissues were fixed in formal saline (10% formalin with 0.9% NaCl) for 72 h at room temperature. The formalin-fixed liver and kidney tissues were dehydrated in ethanol gradient and embedded in paraffin blocks. These blocks were cut into 5 µm thin sections, deparaffinized, rehydrated and stained with hematoxylin and eosin (H&E). The sections were visualized under light microscope (Leica, Wetzlar, Germany) at different magnifications (6.3 and 25 X).

2.12. Determination of blood hematology parameters

The hematological parameters such as red blood cell (RBC), hemoglobin (Hb), monocytes, lymphocytes, eosinophils, basophils, neutrophils, mean corpuscular volume (MCV), mean corpuscular

hemoglobin (MCH), hematocrit (HCT), mean cell hemoglobin concentration (MCHC) and platelets were analyzed by automated hematology analyzer (Sysmax-1800i, Japan).

2.13. Determination of serum biochemical parameters

The serum biochemical analytes such as hepatotoxic biomarkers (total bilirubin, aspartate aminotransferase (AST), alanine aminotransferase (ALT), lactate dehydrogenase (LDH), alkaline phosphatase (ALP) and nephrotoxic biomarkers (creatinine, urea, uric acid, and total protein) with other important physiological biomarker such as Fe, and Hp were estimated through fully automated clinical chemistry analyzer (Rx Daytona, Randox, U.K.).

2.14. Determination of ROS

The liver tissue samples from all animals of each group (G1 to G7) were homogenized in ice-cold TRIS-HCl buffer (40 mM, pH 7.4) separately. All tissue samples were normalized according to estimated protein using bicinchoninic acid (BCA) assay. An equal amount of tissue samples were incubated with 25 μM of DCF-DA for 30 min at 37 °C in dark. The formation of fluorescent products 2, 7 -dichlorofluorescein (DCF) was measured at wavelength of 485 and 520 nm for excitation and emission respectively using microplate reader (FlUOstar Omega, BMG Labtech, Germany).

2.15. RT-PCR for mRNA expression of cytokine and Fe homeostatic biomarkers in hepatocytes

To evaluate the degree of inflammation and APR in the liver, mRNA expression of cytokines TNF-α, IL-6 pro-inflammatory biomarkers MMP-9 and acute phase Hp and hepcidin were measured. Further, the mRNA expression of Fe signaling proteins was evaluated by measuring the gene expression of hepcidin, hephaestin, TFR-1 and Ferroportin (FPN) biomarkers. In beginning, RNA was extracted from liver of all animals of each group G1 to G7 by trizol methods. The extracted pure RNA was estimated and normalized. Furthermore, the cDNA synthesis was performed by using high capacity cDNA reverse transcriptase kit. The equivalent cDNA from G1 to G7 were used for the quantitative q-PCR system "(Thermo Fischer, Rockford, IL, USA). The reaction mixture of RT-PCR was prepared with SYBR Green master mix (Takara, Japan) according to the manufacturer's protocol. All Primers used for mRNA expression of Hp, TNF-α, IL-6, MMP-9, TFR-1, FPN, hepcidin, hephaestin, and β-actin were designed on NCBI website and procured from IDT Ltd, USA. The used β-actin primers act as the internal control. The details of all primers are summarized in Table 1. The threshold cycle numbers (Ct value) in triplicate reactions for each primer were used to calculate relative gene expression in treated samples with respect to the control according to the standard method with [25].

2.16. Western blotting for protein expression of hemolytic biomarkers

To evaluate the alteration of Fe signaling pathway, the protein expression of Hp and hephaestin in liver were performed using western blotting where β-actin was used as an internal control. The frozen liver tissues were homogenized in tissue lysis buffer containing a cocktail of protease and phosphatase inhibitor. The extracted proteins were quantified by BCA method (BCA protein estimation kit; Thermo Fisher Scientific, USA) and normalized according to their protein estimation, simultaneously mixed with 5 X Laemmli buffer and incubated at 90 °C for 30 min after that loaded on 10% gel as progressively performed SDS-PAGE. Afterward, the bands were blotted on PVDF membrane in blotting buffer (14.4 g/L glycine, 3.03 g/L Tris, 20% methanol). The transferred membrane was blocked in 5% bovine serum albumin in PBST for 1 h, followed by incubation for overnight at 4 °C with primary antibody; hephaestin, β-actin and Hp separately. Antibody immobilized membranes were incubated with corresponded HRP-conjoined secondary antibody for 2 h. Finally, the blot was analyzed using an enhanced chemiluminescent substrate (Thermo Fisher Scientific, USA) as stated in the manufacturer's protocol and imaged through gel documentation system (Amersham Imager 600, UK). The expression of proteins was again quantified through densitometry analysis using Image J software (National Institute of Health, Bethesda, MD, USA).

Table 1
Detail of the primer sequence used for real time PCR.

	Primer name		Sequence
1	β-ACTIN	F	GTCCCTGTATGCCTCTGGTC (n = 20)
		R	CTCCAGGGAGGAAGAGGATG (n = 20)
2	Hp	F	CTGGCCTCACCAAGTACCAG (n = 20)
		R	GCAGGGCTAGAACCCATCAG (n = 20)
3	TNF-α	F	CCCATATACCTGGGAGGAG (n = 19)
		R	CTGTCCCAGCATCTTGTG (n = 18)
4	Hepcidin	F	CTCCTGCTTCTCCTCCTT (n = 18)
		R	GGTCAGGATGTGGCTCTA (n = 18)
5	IL-6	F	CTCCCTTACCCACCAACTCC (n = 20)
		R	CTGTCTCGTGTGAGGCTAGG (n = 20)
6	TFR-1	F	GTGGAGGGTCAACGTGGTAG (n = 20)
		R	GGCAGATGCCAAGAGGAGAG (n = 20)
7	Hephaestin	F	TCAGTGGGACTTTCTGTCTTATG (n = 23)
		R	CTTCTTCACTCCAGCTCTACAC (n = 22)
8	MMP-9	F	CTTCTGGCGTGTGAGTTTCCA (n = 21)
		R	ACTGCACGGTTGAAGCAAAGA (n = 21)
9	Ferroportin	F	GGAAACAGAGAGACAGACAG (n = 20)
		R	CTATCACAGGTTCGGGTATG (n = 20)

TFR-1- transferrin receptor-1, Hp- haptoglobin, matrix metalloproteinase-9 (MMP-9), tissue inhibitor of metalloproteinase-2 (TIMP-2), Interleukin-6 (IL-6) and tissue necrotic factor-α (TNF-α).

2.17. Immunohistochemistry (IHC) for expression of anemic biomarkers

For IHC, the 5 μm thick sections of the intestine (duodenum) were rehydrated and processed for antigen retrieval by using citrate-EDTA buffer. Retrieved slides were incubated with blocking buffer (5% BSA) for 1 h to stop the nonspecific binding. Subsequently, slides were incubated for overnight with Heph-primary antibody (hephaestin) at 4 °C, washed and incubated with Alexa fluor 488 for 2 h at room temperature. The unspecific immobilized antibodies were washed with 1 X PBS, and the slides were mounted with fluoroshield DAPI solution and analyzed under the fluorescent microscope (Leica Microsystems, DMLB30S, Wetzlar, Germany) using appropriate filters.

2.18. Statistical analysis

All the data were presented as the mean ± standard deviation (mean ± SD). The statistical analysis of quantitative variables was analyzed by using one-way analysis of variance (ANOVA) followed by the dunnett post hoc test (compare each group with control group for every parameter). Data analysis was carried out by using Graph pad prism software version 5.1 (GraphPad Software, La Jolla, CA, USA). All the comparisons were evaluated at 5% ($p < 0.05$) level of significance.

3. Results

3.1. Characterization of c-ZnO NPs and b-ZnO NPs

The functionalization of the GG by PAm polymer was initiated by $KMnO_4$ and oxalic acid in aqueous media as shown in Fig. 1(A). PAm-g-GG proffered the spacer to regulate the *in-situ* synthesis of ZnO NPs along the compatibility, hydrophilicity and surface charge neutrality.

The functional group's analysis of GG, PAm-g-GG and c-ZnO NPs were done by using ATR-FTIR spectra (Fig. 1(A)). The PAm-g-GG spectrum has additional peaks regarding N—H stretching, amide-I (CO

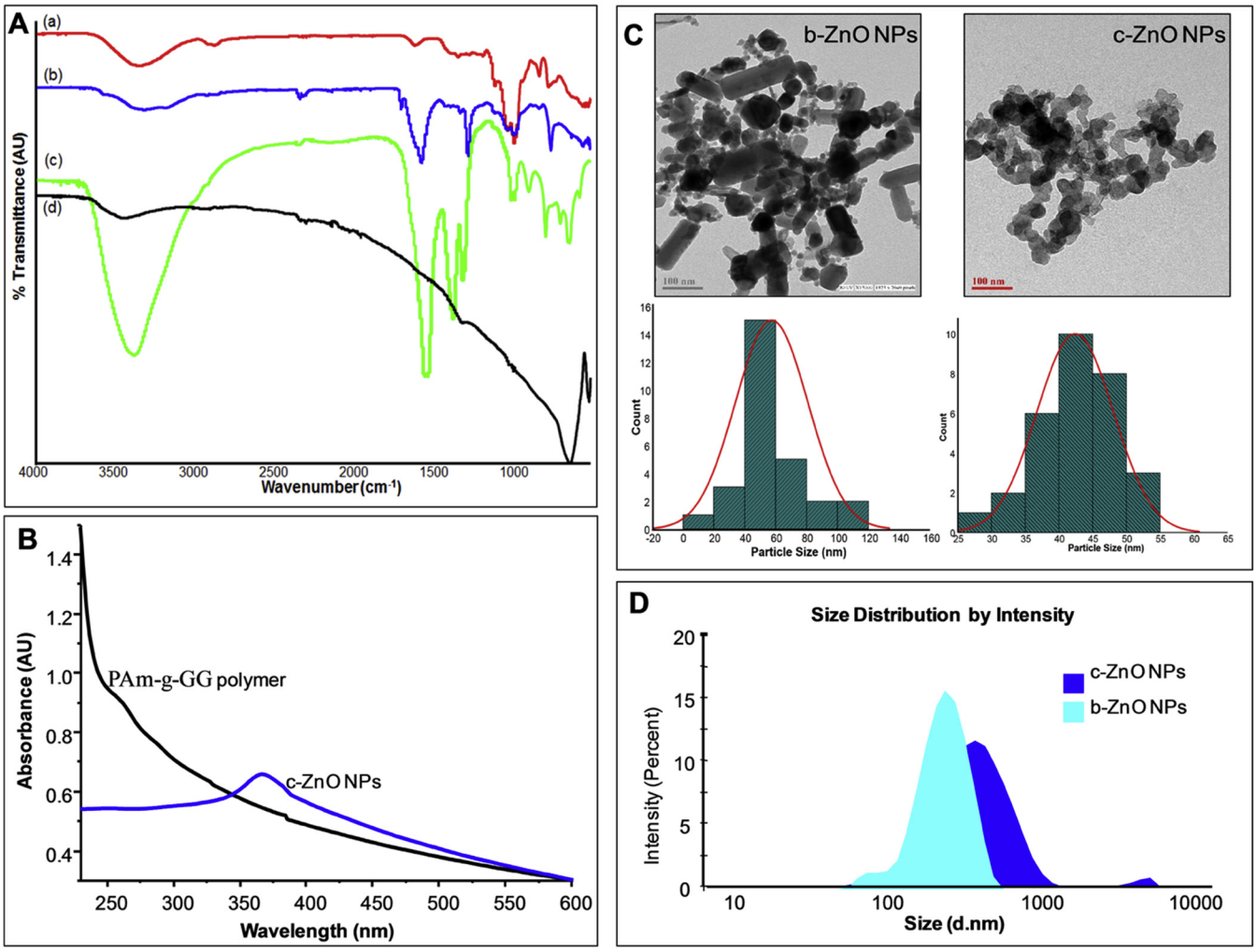

Fig. 1. A: ATR-FTIR spectra of GG, Pam-g-GG, c-ZnO and b-ZnO NPs, B: Absorbance spectra of c-ZnO and b-ZnO NP, C: TEM analysis along with histogram of both NPs: b-ZnO NPs and c-ZnO NPs, D: A: Variance in hydrodynamic diameter of c-ZnO and b-ZnO NPs.

stretching) and amide–II (N—H bending) at 3205, 1670 and 1580 cm^{-1}, respectively. The peak at 1424 cm^{-1} has denoted C—N stretching vibrations of the amide group. An absorption band at 2925 cm^{-1} is referred to the C—H stretching of CH_2 groups of GG matrix in all spectra. The GG, PAm-g-GG and c-ZnO NPs spectra have a glucosidic (C—O—C) bond and primary alcohol C—O stretching vibrations corresponding to GG moiety, respectively at 1141 and 1029 cm^{-1} which further promised to successful grafting on GG. Further, Zn-O stretching vibration has been seen at 490 cm^{-1} in the c-ZnO NPs which resemble b-ZnO NPs spectrum. Fig. 1(B) has illustrated the UV–vis absorbance of c-ZnO and b-ZnO NPs.

Fig. 1(C) has shown TEM images of b-ZnO and c-ZnO NPs with the corresponding histogram respectively. Image of b-ZnO NPs has shown irregular particles shape with a range of 10–60 nm while the c-ZnO NPs are globular with predominately 20–45 nm which advocating the applicability of PAm grafting on GG to direct shape and size of NPs. The DLS plot (Fig. 1(D)) of b-ZnO and c-ZnO NPs has shown the hydrodynamic diameter of respective NPs which are exhibited in range of 255 nm (b-ZnO NPs) and 396.1 nm for c-ZnO NPs. Zeta potential of b-ZnO and c-ZnO NPs were −31 and −1 mV respectively.

3.2. Dissolution Properties of ZnO in dose formulation and in biofluids

The stability of ZnO NPs and release of Zn^{2+} in dosing medium was assessed in samples incubated for 24 h using AAS. The concentration of released Zn^{2+} was found to be very low (< 1% of total concentration) as shown in Fig. 3(A).

The solubility of ZnO nanoparticles was also evaluated in simulated gastric, mouse extracted gastric, and serum fluids in order to elucidate their biological fate when administered orally. It was found that 12.04% and 12.22% of b-ZnO NPs and c-ZnO NPs dissolved into zinc ions in simulated gastric fluid, however, 22.24% and 18.24% in extracted gastric fluids, respectively (Table 2). Meanwhile, the respective solubility of b-ZnO and c-ZnO were 13.27% and 7.83% in serum conditions (Table 2).

Table 2
Dissolution property of ZnO NPs in different bio-fluid.

Sample	Test system	Dissolved Fraction (%)
b-ZnO NPs	Water	0.125 ± 0.001
	Simulated Gastric Fluid	12.04 ± 1.80
	Extracted Gastric Fluid	22.24 ± 2.22
	Serum	13.27 ± 5.26
c-ZnO NPs	Water	0.02 ± 0.001
	Simulated Gastric Fluid	12.22 ± 2.18
	Extracted Gastric Fluid	18.24 ± 0.85
	Serum	7.83 ± 2.52

c-ZnO NPs-capped Zinc oxide nanoparticles, b-ZnO NPs-bared Zinc oxide nanoparticles.

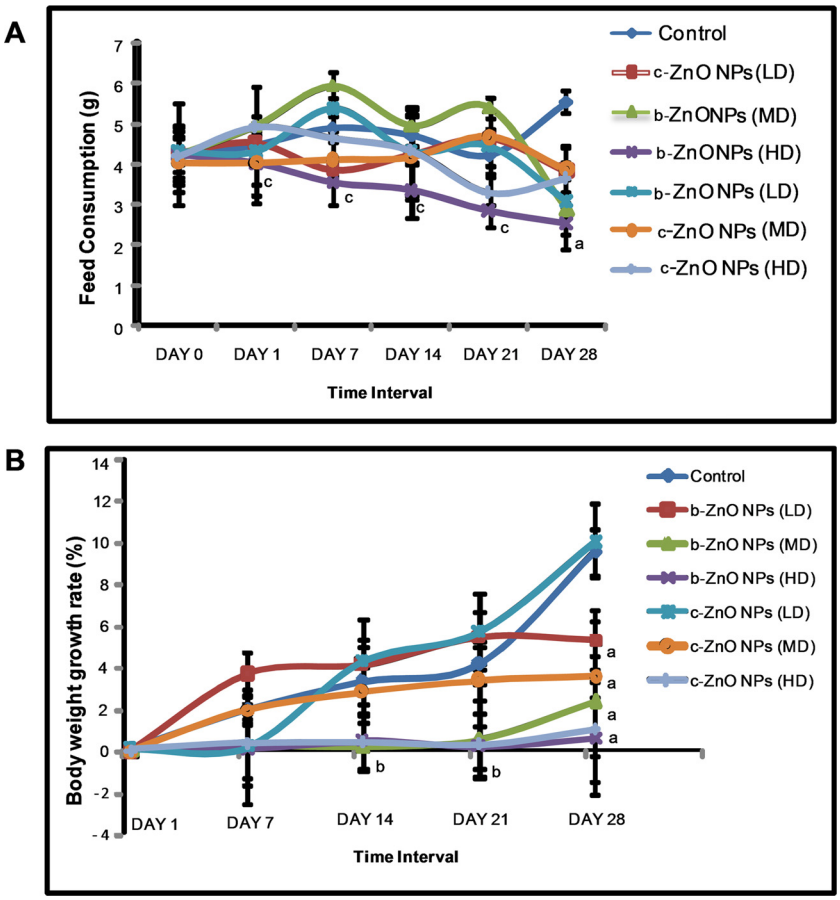

Fig. 2. A and B; Food consumption and % body weight growth of both NPs treated groups.
Data were represented as mean ± SD; n = 10 animals per groups, a, b and c denotes statistically significant differences at $p < 0.001$, $p < 0.01$ and $p < 0.05$ as compared to control respectively.
NPs- Nanoparticles; c-ZnO NPs-capped Zinc oxide nanoparticles, b-ZnO NPs-bared Zinc oxide nanoparticles, LD- low dose, HD- high dose.

3.3. Effect of NPs treatment on body and organ weight of animals

There was no mortality observed in any group of experimental animals. The animals of high dose groups (G2 and G5) were showed significant falls off in feed intake and body weight growth rate as shown in Fig. 2.

3.4. Accumulation of Zn after oral treatment

The measurement of accumulated Zn in the liver, kidney, and plasma of treated animals was carried out by AAS analysis. A dose-dependent significant higher accumulation in tissue was found in b-ZnO NPs in comparison to c-ZnO NPs after repeated oral administration. Animals treated with 300 mg/kg of b-ZnO NPs, the Zn concentration in liver and kidney was found to be higher ($p < 0.001$ and $p < 0.05$) 48.2 ± 6.07 µg/g and 71.16 ± 3.16 µg/g but slight lesser in c-ZnO NPs ($p < 0.05$; 45.06 ± 3.01 and 51.08 ± 4.36 µg/mg wet tissue respectively) as compared to control. The concentration of Zn in plasma was significantly higher in c-ZnO NPs ($p < 0.001$; 88.95 ± 6.70) in contrast to b-ZnO NPs ($p < 0.01$; 50.54 ± 7.49) as presented in Fig. 3(C). The result indicated the higher Zn accumulation in tissue with low circulation in the blood of b-ZnO treated groups as compared to c-ZnO NPs.

In the biological environment and during oral treatment, ZnO NPs may release Zn^{2+} that can significantly contribute to its toxicity. To address this issue, we did Triton X-114 (TX-114)-based cloud point extraction (CPE) to differentiate the amount of ZnO NPs and Zn^{2+} in liver and kidney tissue. The result indicated 60–65% zinc in tissue is ionic form and one third part 30–35% is in non-ionic form. Thus according to finding, ZnO NPs shows maximum dissolution property (higher Zn^{2+}) during oral administration (Fig. 3(B)).

3.5. Evaluation of Cellular defects and tissue damage

The ultra-structural analysis of liver and kidney tissues was performed by TEM to check the comparative effect of b-ZnO and c-ZnO NPs on cellular organelles. TEM analysis showed that the significant non-ionic part of ZnO NPs also accumulated in hepatocyte cells (Fig. 4) and kidney tissue (Fig. 5). The accumulated object in tissue was Zn was confirmed by TEM images on CCD camera.

The cellular organelles of the liver such as endoplasmic reticulum (ER) were highly degraded in b-ZnO as compared to c-ZnO NPs that pointing loss of transportation and absorption of several micronutrient, minerals, and hormones required for proper functioning of the cells. There was increased hepatic cytoplasmic vacuolization and loss of hepatocytic organelles with degenerated mitochondrial cristae were also observed in both high dose treated groups (G2 and G5) but found comparably higher in b-ZnO NPs (Fig. 6).

TEM analysis of kidney tissue was indicated the cellular internalization of NPs in nucleus, mesangial cell and basement membrane (Fig. 5) that induced the deformities. The podocyte cells of glomeruli showed irregular formatting and the lumen showed higher seepage of proteinaceous material. The podocyte swelling and deformities in their processing are common in NPs treated group. The induced lesions were found in both NPs treated groups but their changes were significantly high in b-ZnO NPs treated animals as shown in Fig. 7.

3.6. Histopathological evaluation

The histology of liver and kidney tissue (Figs. 8 and 9) has shown the lesions in a dose-dependent manner after treatment of both types of NPs, while more lesions were found in b-ZnO NPs. In liver tissue, the high dose of b-ZnO NPs shows hepatocyte degeneration with mild congestion, further the karyonectic in nucleus cells were also

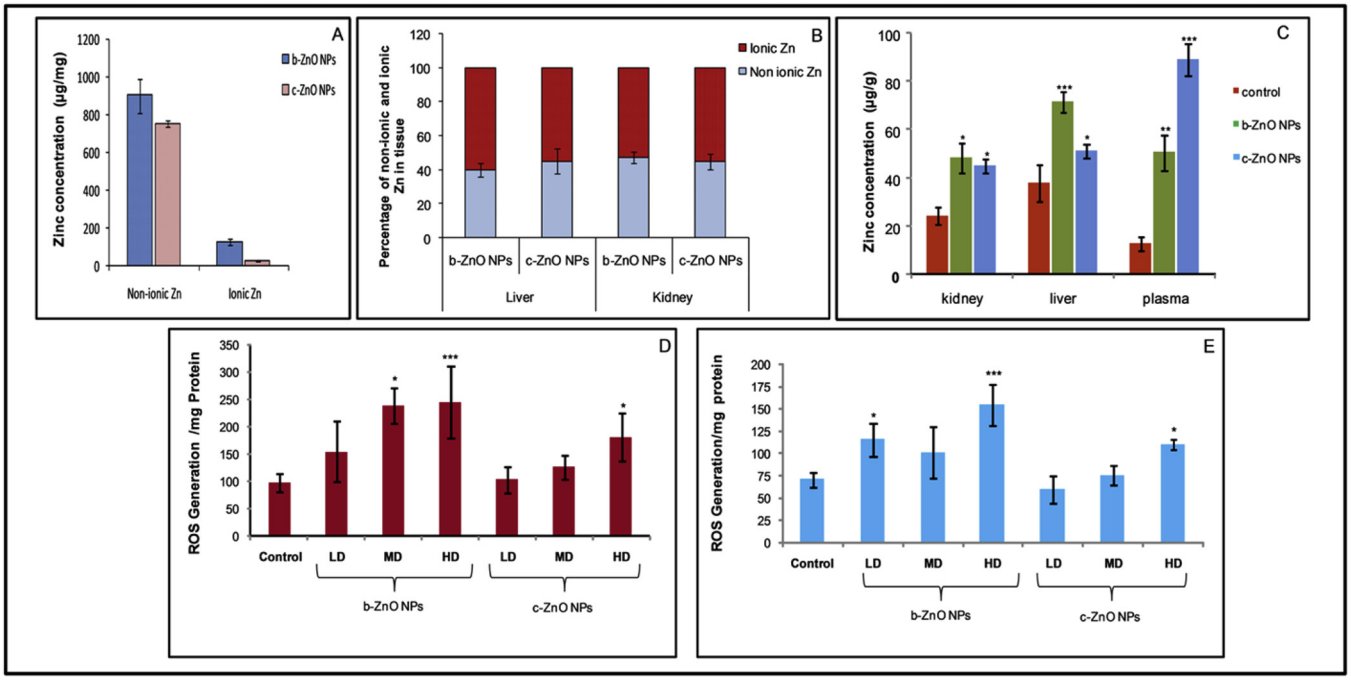

Fig. 3. Effect of b-ZnO and c-ZnO NPs treatment. (A) Dissolution property (release of ion) of both ZnO NPs in dose formulation up to 24 h from the time of dose preparation at pH 7.4 (normal biological pH), n = 5 number of repeats, (B) Percentage of accumulated ionic and nonionic zinc in liver and kidney after 28 days repeated treatment at the dose of 300 mg/kg, (C) Accumulation of zinc in liver, kidney and plasma at the dose of 300 mg/kg after 28 days repeated treatment assessed by AAS, (D) ROS generation in liver, (E) ROS generation in kidney.
NPs-Nanoparticles; c-ZnO NPs-capped Zinc oxide nanoparticles, b-ZnO NPs-bared Zinc oxide nanoparticles, LD- low dose, HD- high dose.
Data were represented as mean ± SD; n = 5 animals per groups. *, **, *** denotes statistically significant differences at $p < 0.05$, $p < 0.01$, and $p < 0.001$ as compared to control respectively.

noticeable. At a mid dose of b-ZnO NPs the hepatocytes congestion and degenerative changes were also detected. The c-ZnO NPs at higher dose also show moderate hepatocyte degeneration but less as compared to b-ZnO NPs. The lower dose groups of each NPs is not shown any major deformities, on the whole, the higher lesions were found in b-ZnO NPs as compared to c-ZnO NPs (Fig. 8).

In the kidney, the histopathological evaluation was performed to see the lesions in nephritic cells after 28 days repeated oral administration

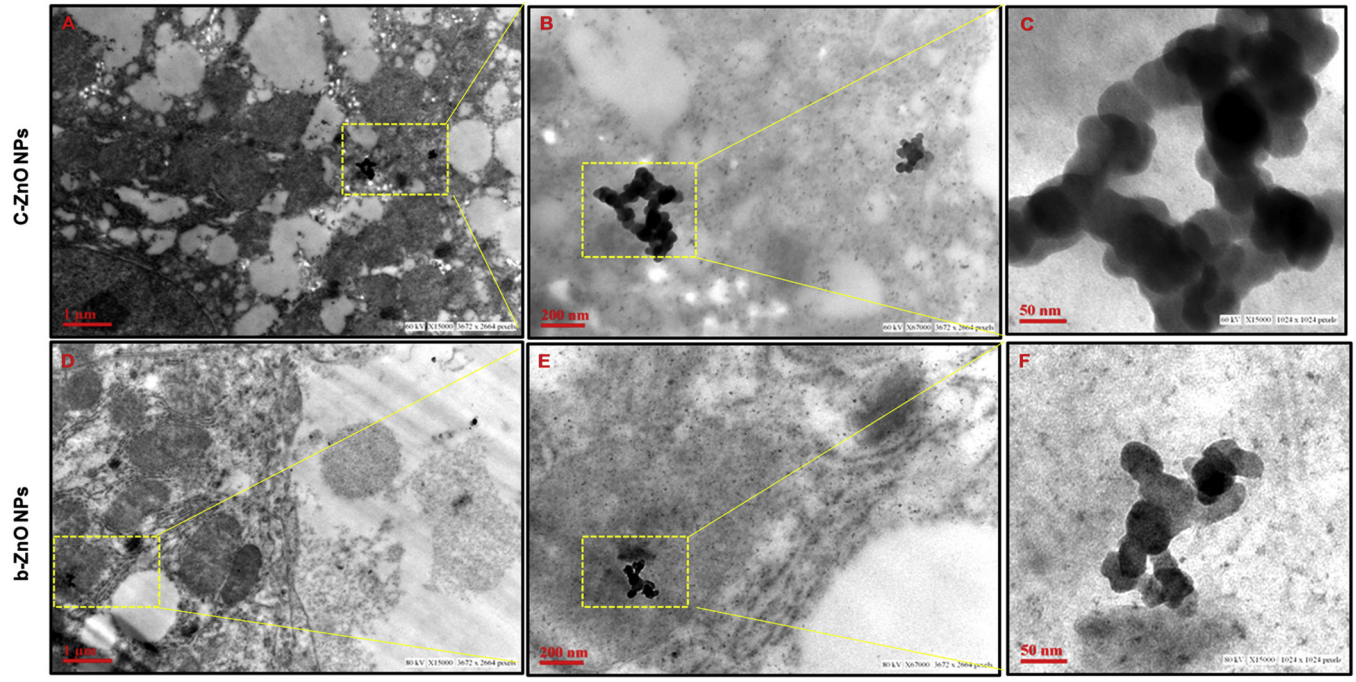

Fig. 4. Accumulation and internalization of c-ZnO and b-ZnO NPs in liver. TEM images of unstained liver sections showing accumulation of NPs after 28 days repeated oral dose of 300 mg/kg. Inset view shows image of ZnO NPs by side mounted CCD camera. Image A, B and C represent the internalization c-ZnO NPs in hepatocyte cells while D, E and F represent internalization and accumulation of b-ZnO NPs in hepatocye cell.

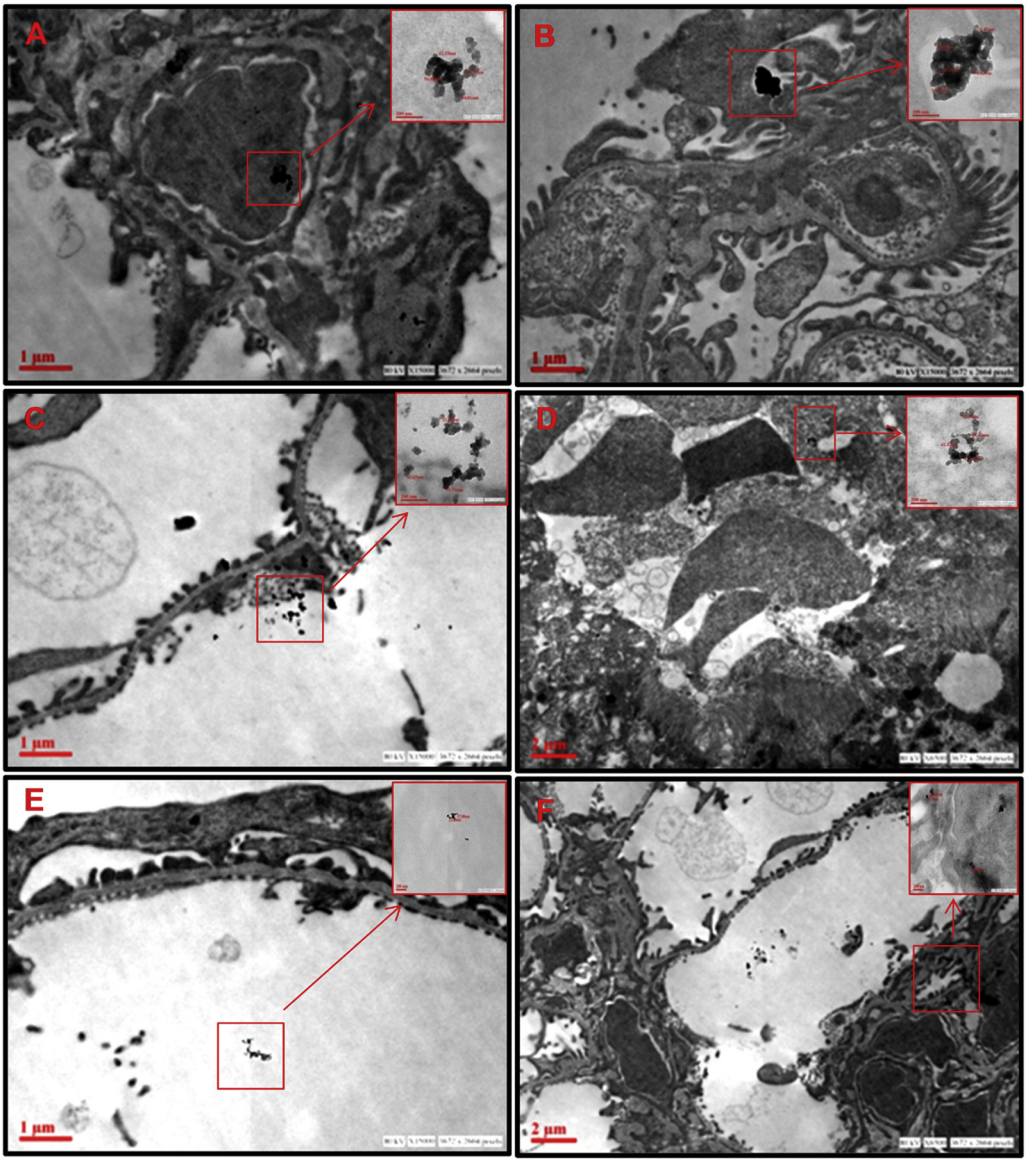

Fig. 5. Accumulation of c-ZnO and b-ZnO NPs in various parts of the kidney, TEM images of unstained kidney sections showing accumulation of NPs in various parts after 28 days repeated oral dose of 300 mg/kg. Inset view shows image of ZnO NPs by side mounted CCD camera. Image A, B and C represent b-ZnO NPs while D, E and F represent c-ZnO NPs. (A) b-ZnO NPs in nucleus. (B) b-ZnO NPs in mesangial cells. (C) b-ZnO NPs membrane near lumen. (D) c-ZnO NPs in lumen. (E) c-ZnO NPs near glomeruli membrane. (F) c-ZnO NPs in mesangial cell.

with c-ZnO and b-ZnO NPs. The b-ZnO NPs at high dose show renal tubular degeneration, higher eosinophilic proteinaceous material deposition in PCT lumen, the glomeruli were also damaged as seen in Fig. 9. The glomeruli were swelled with degenerative changes. Further, the eosinophilic proteinaceous material deposition in the tubular lumen in c-ZnO NPs at the dose of 300 mg/kg, on the other hand at mid dose the b-ZnO NPs show mild vascular degeneration. At lower dose, the mildly vascular generation was seen in b-ZnO NPs in contrast low adverse effects were seen in c-ZnO NPs at a low dose.

3.7. Alteration in serum nephrotoxic and hepatotoxic biochemical parameters

The serum biochemical parameters; AST, ALT, ALP, LDH, creatinine urea, and uric acid were accreted significantly ($p < 0.001$) in the high dose of b-ZnO NPs treated group (G2) as analogized to control (G1). In high dose, c-ZnO NPs treated group (G5), the level of ALT, uric acid and creatinine were increased but less significant ($p < 0.01$). The mid dose of b-ZnO NPs showed an elevated level of ALP and creatinine ($p < 0.05$). The other groups were not showed any significant changes (Fig. 10).

Moreover, the significant reduction of Fe and Hp level were also recorded in high dose treated groups (G2 and G5) as presented in Figs. 10 and 11. The level of serum Fe and Hp were decreased significantly in G2 ($p < 0.001$) of b-ZnO NPs and G5 group of c-ZnO NPs ($p < 0.01$) as compared to control. The mid and low dose groups of b-ZnO NPs (G3 and G4) also showed a significant ($p < 0.01$) reduction in Fe and Hp (Fig. 10).

3.8. Alteration in blood hematology parameters

The mean hematological parameters of G1 toG7 groups are presented in Fig. 11. The statistically significant reduction in RBC, Hb, HCT, MCH, MCHC, and platelets were found in a high dose of b-ZnO NPs treated group (G2) animals in compared to control (G1). The high dose c-ZnO NPs treated group (G5) animals have shown significantly declined level of RBC, Hb, HCT and MCH as compared to control but very less ($p < 0.05$) as compared to G2 (< 0.01), as presented in

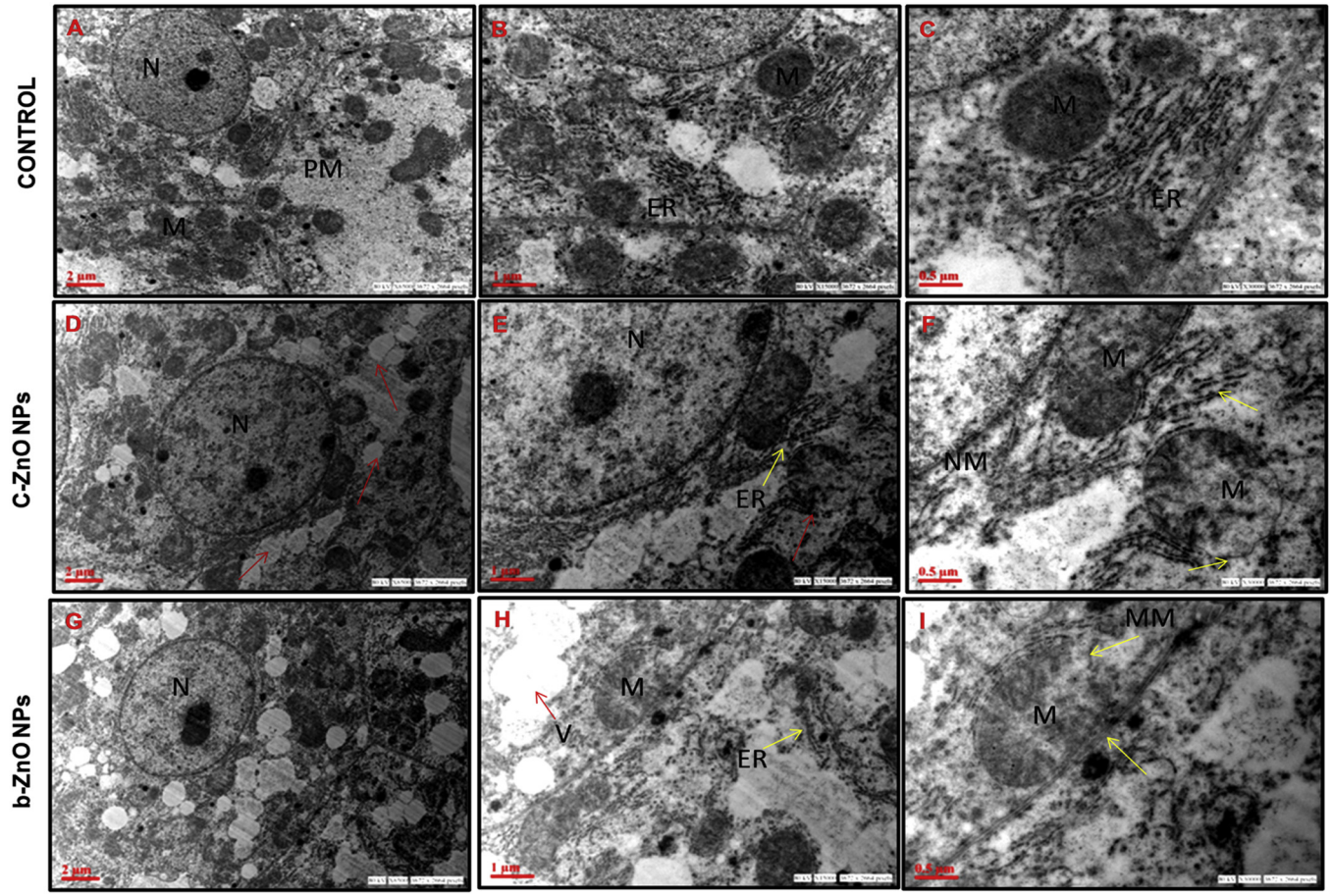

Fig. 6. ZnO NPs treatment causes damage to the liver tissue, the tissue were collected after 28 day repeated oral administration of c-ZnO and b-ZnO NPs at the dose of 300 mg/kg. Representative transmission electron microscopic images are shown. (A, B and C) Control hepatocyte cells at 15,000× and 30,000× magnification. (D and E) Sections of animals treated with c-ZnO NPs at different area. 15,000× magnification. (F) Sections of animals treated with c-ZnO NPs. 30,000× magnification. (G and H) Sections of animals treated with b-ZnO NPs at different area. 15,000× magnification. (F) Sections of animals treated with b-ZnO NPs. 30,000× magnification.

NPs-Nanoparticles; c-ZnO NPs-capped Zinc oxide nanoparticles, b-ZnO NPs-bared Zinc oxide nanoparticles, ER- endoplasmic reticulum, M- mitochondria, N- nucleus, NM- nuclear membrane, PM- plasma membrane, V-vacuole. Arrow shows the damages in relevant region.

Fig. 11.

3.9. Measurement of induced oxidative stress

The exposure of ZnO NPs in animals was associated with increased ROS production as assessed by DCF-DA assay (Fig. 3(D and E)). A remarkable high production of free radicals was found in the liver and kidney at the high dose of b-ZnO (G2) (244.93 ± 66.19 and 155.0 ± 23.85 at $p < 0.001$) and c-ZnO NPs (G5) (180.96 ± 43.13 and 109.98 ± 5.46 at $p < 0.05$) as compared to control (G1).

3.10. Alteration of mRNA expression of cytokine, inflammatory, and APR biomarkers

A quantitative RT-PCR was done for mRNA expression of cytokines and pro-inflammatory biomarkers such as IL-6, MMP-9, Hp and TNF-α in liver tissues of b-ZnO (G2, G3 and G4) and c-ZnO NPs (G5, G6, and G7) (Fig. 12(B)). A significant higher ($p < 0.001$) gene expression of IL-6 was found in the G2 and G3 group of b-ZnO NPs (1.8 ± 0.26 and 1.56 ± 0.007) fold) while 1.19 ± 0.01 folds expression was seen in the G5 group of c-ZnO NPs ($p < 0.05$). The MMP-9 genes expressions were significant increased ($p < 0.001$) in G2 (3.19 ± 0.53), G3 (2.76 ± 0.49), G4 (2.66 ± 0.26) of b-ZnO NPs while less significant in c-ZnO group ($p < 0.001$, $p < 0.01$, $p < 0.05$) in G5 (2.48 ± 0.1), G6 (2.3 ± 0.3), G7 (1.78 ± 0.23) groups respectively as compare to control. The expression of TNF-α has significantly elevated in the G5 group of c-ZnO NPs (1.82 ± 0.34; $p < 0.001$) rather than G2 and G3 groups of b-ZnO NPs showed significantly higher expression ($p < 0.001$; 3.16 ± 0.26 and 1.9 ± 0.23 fold respectively).

Whether the acute phase protein (APP) such as hepcidin and Hp were increased their expression in b-ZnO NPs as compared to c-ZnO NPs. The expression of Hepcidin elevated in fold ($p < 0.001$) in G2 (4.18 ± 0.08), G3 (2.18 ± 0.1) of b-ZnO NPs, whereas, G5 and G6 of c-ZnO NPs showed elevation (1.49 ± 0.01 and 1.29 ± 0.1 fold) at the significant level $p < 0.001$ and $p < 0.05$ respectively that is less significant than b-ZnO NPs. Another acute phase biomarker Hp gene expression was significantly increased in G2 ($p < 0.001$), G5 ($p < 0.01$) and G6 ($p < 0.01$) in fold 3.38 ± 0.13, 1.75 ± 0.06, and 1.08 ± 0.08 respectively. Consequently, the outcome has revealed that the mRNA expression was greatly altered in b-ZnO as compared to c-ZnO NPs that indicated the progression of inflammation and a condition of APR were higher in b-ZnO NPs (Fig. 12(B)).

3.11. The mRNA expression of APR linked Fe signaling biomarkers

The mRNA level of Fe signaling biomarkers such as hepatic hephaestin, TFR-1 and FPN were assessed by RT-PCR analysis (Fig. 12(B)). A dose-dependent alteration of all mRNA gene level was seen in all groups with maximum changes in both G2 and G5 groups as compared to G1. The Fe transporting gene hephaestin was significantly decreased

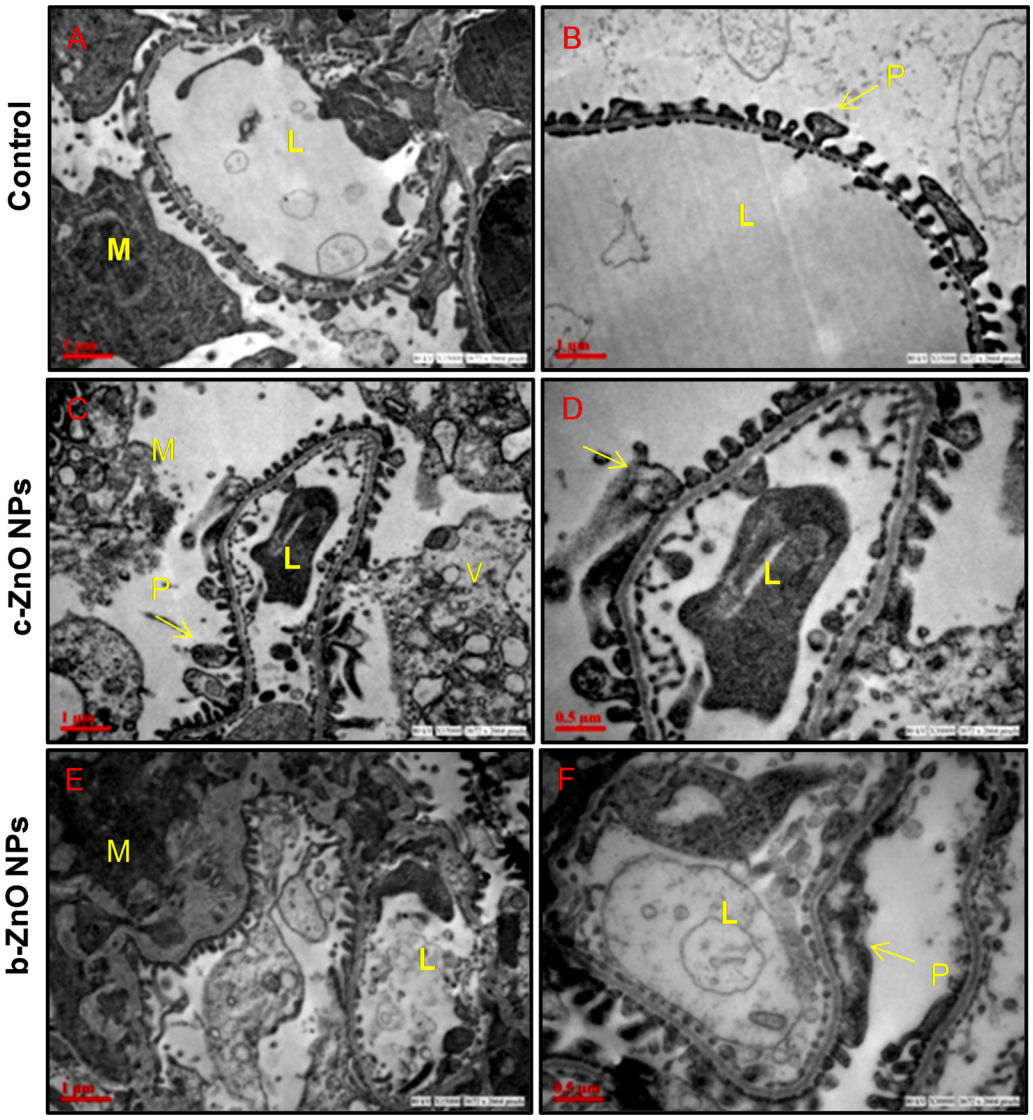

Fig. 7. ZnO NPs treatment causes damage to glomerular region of kidney, kidney were collected after 28 day repeated oral administration of c-ZnO and b-ZnO NPs at the dose of 300 mg/kg. Representative transmission electron microscopic images are shown. (A and B) Control glomerulus at 15,000× magnification. (C) Sections of animals treated with c-ZnO NPs. 15,000× magnification. (D) Sections of animals treated with c-ZnO NPs. 30,000× magnification. (E) Sections of animals treated with b-ZnO NPs. 15,000× magnification. (F) Sections of animals treated with b-ZnO NPs. 30,000× magnification.
NPs- Nanoparticles; c-ZnO NPs -capped Zinc oxide nanoparticles, b-ZnO NPs-bared Zinc oxide nanoparticles, Mesangial cells, N- nucleus, NM- nuclear membrane, PM- plasma membrane, P- podocyte. Arrow shows the podocyte foot process.

in all treated groups but the decreasing pattern in G2, G3, and G4 of b-ZnO NPs was (0.11 ± 0.00, 0.26 ± 0.05, 0.71 ± 0.07) more significant ($p < 0.001$) while G5 (0.38 ± 0.00), G6 (0.56 ± 0.07), and G7 (0.79 ± 0.04) of c-ZnO NPs showed less significant $p < 0.001$, $p < 0.01$, $p < 0.05$ respectively. The Fe transporting receptor gene FPN was significantly declined in G3 ($p < 0.001$; 0.40 ± 0.04) and G2 ($p < 0.001$; 0.34 ± 0.02) groups of b-ZnO NPs while in c-ZnO NPs only in G5 group ($p < 0.001$; 0.67 ± 0.06). Further, the expression of TFR-1 was significantly increased ($p < 0.001$; 1.81 ± 0.05 fold) in b-ZnO NPs high dose group (G2), other groups showed non-significant increases. The overall finding of mRNA expression was denoted that the b-ZnO NPs having the higher observable significant alteration in homeostasis biomarkers as compared to control.

3.12. Changes in Fe homeostatic biomarkers 'hephaestin and haptoglobin' protein expression in liver: Western Blotting

The hepatic Hp and hephaestin protein levels were assessed in the liver by western blot analysis (Fig. 12(A)). Dose-dependent significant increases in expression were seen in Hp proteins in all groups with the maximum finding in b-ZnO in contrast to c-ZnO NPs. Whereas, the expression of hephaestin protein were significantly declined in all treated groups (G2 to G7) as compared to control (G1). The decreasing pattern of hephaestin and increasing pattern of Hp were significantly altered in b-ZnO NPs. Further the quantitative measurement through densitometry showed the significant decreases in expression (fold) of hephaestin in G2 ($p < 0.001$; 0.31 ± 0.05), G3 ($p < 0.001$; 0.57 ± 0.06), G4 ($p < 0.001$; 0.55 ± 0.03) of b-ZnO NPs while the decreasing pattern were less significant in c-ZnO NPs groups that is G5 ($p < 0.001$; 0.62 ± 0.06), G6 ($p < 0.001$; 0.53 ± 0.05), G7 ($p < 0.01$; 0.47 ± 0.03). Whereas, the significant increased in expression ($p < 0.001$) of Hp in G2, G3, and G4 were 3.41 ± 0.05, 3.68 ± 0.10, 3.84 ± 0.02 of b-ZnO NPs and 4.78 ± 0.16, 4.30 ± 0.15, 4.10 ± 0.084 for G5, G6, G7 of c-ZnO NPs groups respectively.

3.13. IHC for expression of Fe homeostatic biomarkers 'hephaestin' in the intestine

The IHC analysis in duodenum was also manifested the decreasing level of hephaestin in ZnO NPs treated groups than the control (Fig. 13). Since, the expression pattern in b-ZnO (G2, G3 and G4) is found to be significantly lower than c-ZnO NPs (G5, G6, and G7) in a dose-dependent manner. The quantitative analysis through RGB (Image J) indicated the significant increased in expression ($p < 0.01$) for G2 (13.4 ± 5.83) and G5 (15.36 ± 3.71), while the low dose group of b-ZnO NPs G4 (18.02 ± 4.13) also showed significantly reduced level ($p < 0.05$) as compared to control (29.78 ± 5.83). The expression of

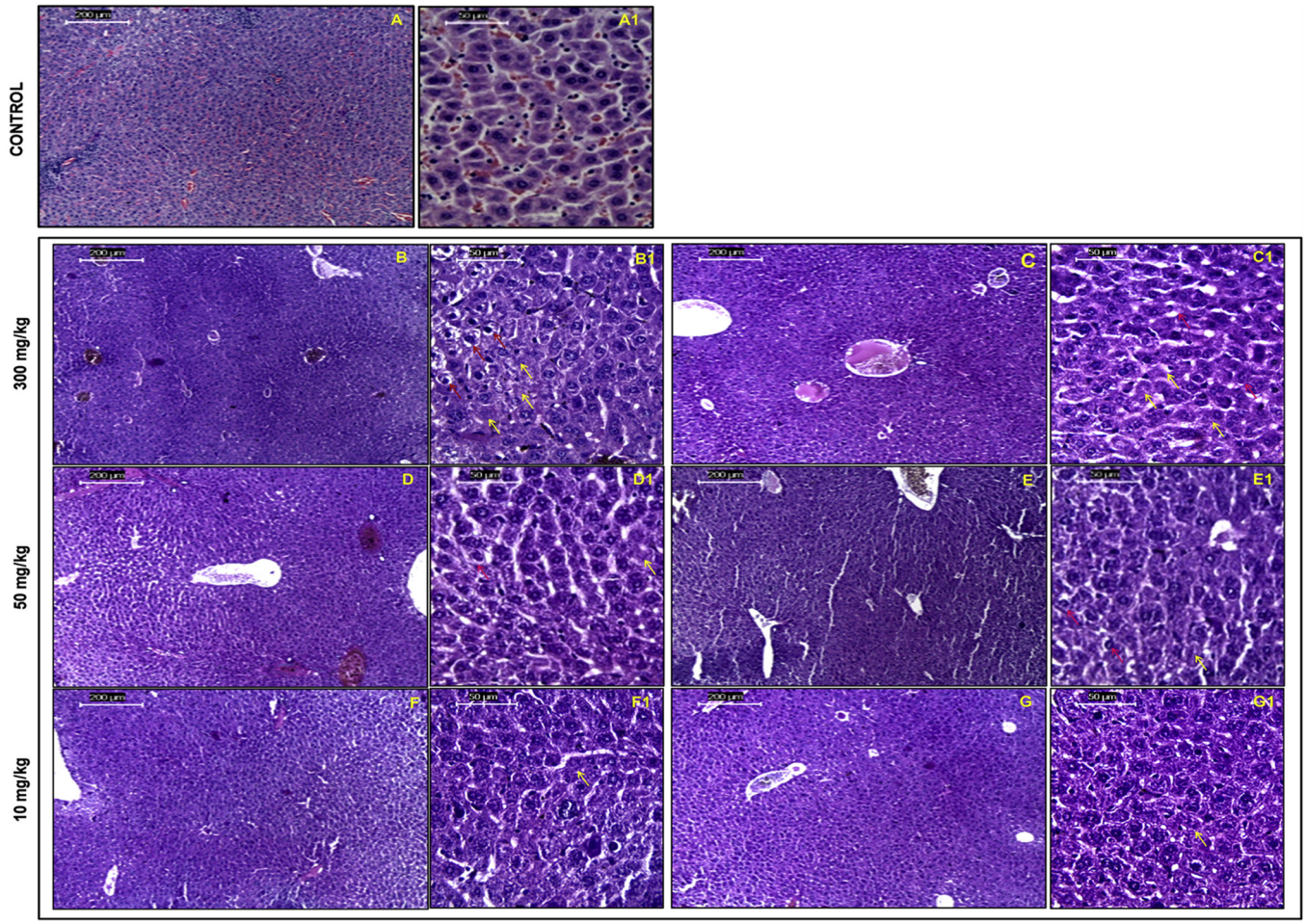

Fig. 8. Histopathological evaluation of liver tissue of female Swiss mice after 28 days repeated oral administration with c-ZnO and b-ZnO NPs (H&E Stain: A to G-total magnification 100×; A1 to G1- total magnification 400×) (A and A1): no changes show in control; (B and B1): show hepatocytes degeneration, karyotectic nucleus, in b-ZnO NPs at dose of 300 mg/kg; (C and C1): moderate hepatocyte degeneration in c-ZnO NPs at dose of 300 mg/kg; (D and D1): show degenerative changes in hepatocytes (b-ZnO NPs-50 mg/kg); (E and E1): Image showing congestion (c-ZnO NPs-50 mg/kg); (F and F1): mildly hepatocyte degeneration (b-ZnO NPs-10 mg/kg); (G and G1): no major changes in c-ZnO NPs (10 mg/kg).
NPs- Nanoparticles, c-ZnO NPs-capped Zinc oxide nanoparticles, b-ZnO NPs-bared Zinc oxide nanoparticles. Red arrow- hepatocyte degeneration, yellow arrow-congestion in cells.

hephaestin in the duodenum of intestine plays a critical role for Fe uptake from intestinal lumen to circulation.

4. Discussion

Nanoscale ZnO is widely exploited in various industrial, commercial, biomedical and household fields due to emerging properties. With expanded uses of ZnO NPs containing products, it is expected that the exposure may increase from previously reported daily intake of Zn, maximum (15 mg/day) in humans [26,27]. The recommended doses of Zn in pregnancy and during childhood diarrhea are 15 mg/day and 10 mg/day respectively [27]. Due to its relative safety as compared to other NPs, short-term studies at low doses have shown less adverse effects. However, there is limited long-term studies in animal systems have been reported, especially their metabolic effect on the nutritional surveillance at the molecular levels. ZnO NPs have a strong affinity for sulfur rich proteins and amino acids such as metallothionine leading to their alterations and even precipitation. Nowadays, surface modification is one of the strategies used to prevent or regulate these attachments to biological molecules. Therefore, the objective of the present study is to design surface engineered ZnO (c-ZnO) NPs that alleviated the APR interlinked Fe signaling by reducing the toxicity. The synthesis and desired modifications of c-ZnO NPs was successfully verified through functional group analysis (Fig. 1(A)). The observed absorbance band at 366 nm in UV–vis spectra has to advocate 3.38 eV band gap energy between valance and conduction band of ZnO NPs (Fig. 1(B)) [28]. The TEM analysis demonstrated that c-ZnO NPs have defined ripening owing to the presence of polymeric capping which regulating their crystal growth whereas, commercial b-ZnO NPs having irregular, shape and size which might be due to lack of any stabilizing agent (Fig. 1(C and D)). The results obtained through DLS indicate an increased hydrodynamic size than their primary particle size as evidenced through TEM. It is observed due to the property of agglomeration of NPs in suspension. According to DLS data, aggregation readily occurs in order to reduce their high surface energy and they tend to attract each other resultant form a clump. The hydrophilic polymer moiety around the c-ZnO NPs justified the higher hydrodynamic size than the bared.

To analyze the adverse effect of ZnO NPs after surface modification, sub-acute oral toxicity study was conducted in Swiss mice at the dosage of 10, 50 and 300 mg/kg body weight, furthermore the interlinked Fe homeostasis were also emphasized. Systemic Fe is antagonistically depended on Zn concentration during exposure for long periods [29]. In case of oral exposure, a large number of factors such as variation in pH of gastrointestinal tract, digestive hydrolyzes, and interaction with various food materials are influenced the amount of particles that will be absorbed and release in bloodstream. The absorbed NPs and their

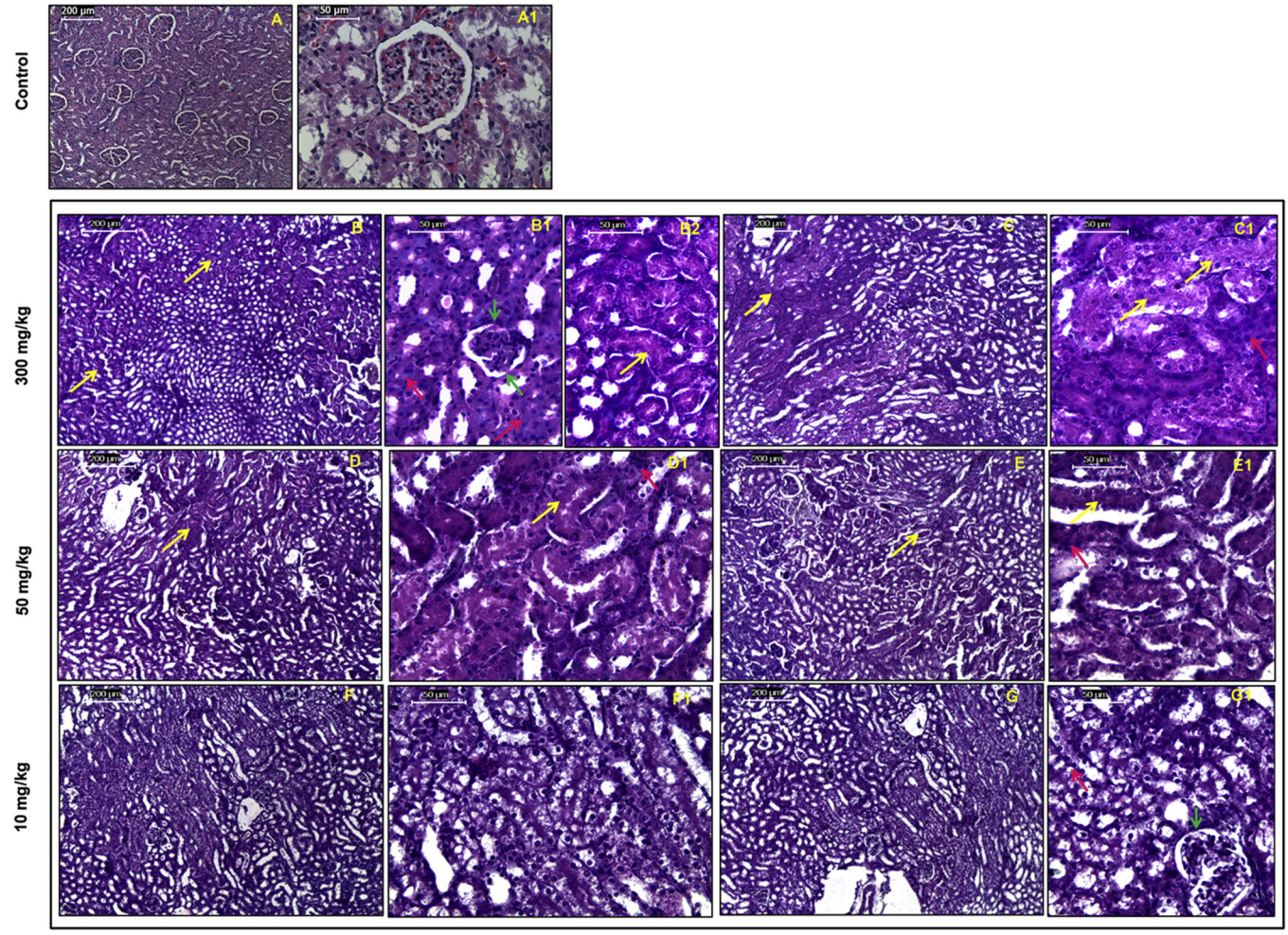

Fig. 9. Histopathological evaluation of kidney tissue of female Swiss mice after 28 days repeated oral administration with c-ZnO and b-ZnO NPs (H&E Stain: A to G- total magnification 100×; A1 to G1- total magnification 400×) (A and A1): no changes show in control; (B, B1, and B2): show renal tubular degeneration, eosinophilic protenaceous material deposition in tubular lumen in b-ZnO NPs at dose of 300 mg/kg; (C and C1): eosinophilic proteinaceous material deposition in tubular lumen in c-ZnO NPs at dose of 300 mg/kg; (D and D1): show mild vascular degeneration (b-ZnO NPs-50 mg/kg); (E and E1): Image showing DCT damages (c-ZnO NPs-50 mg/kg); (F and F1): mildly vacular degeneration (b-ZnO NPs-10 mg/kg); (G and G1): same changes with low effect in c-ZnO NPs (10 mg/kg).
NPs- Nanoparticles; c-ZnO NPs-capped Zinc oxide nanoparticles, b-ZnO NPs-bared Zinc oxide nanoparticles, LD- low dose, HD- high dose.
Arrow: Red-vascular degeneration, yellow-eosinophilic proteinaceous material deposition, green-damages in glomeruli.

ions are highly reactive with the biological molecule and may get accumulate in most common target organ liver and kidney. Recently, Li-Jing et al., has found a significant Zn accumulation in the liver of ZnO NPs treated mice [30]. Here, TEM and AAS analysis were indicated higher accumulation of Zn in liver and kidney tissues after treatment of b-ZnO, where c-ZnO NPs were highly circulated in bloodstream and showed less accumulation in tissue might be due to their surface neutrality. The nature of accumulated Zn in targeted tissues, whether it is solute or NPs matrix was confirmed by cloud point extraction (CPD). The result manifested that 60–65 % Zn was accumulated as solute (ionic) and remaining 30–35 % was found as particulate matter (non-ionic) that was further seen by TEM analysis (Fig. 3). During oral exposure, the ratio of ionic and NPs matrix in accumulated Zn might depend on the dissolution of NPs in the biological fluid (gastrointestinal fluid and serum). The previous report has been demonstrated that the ZnO NPs were partially dissolved in simulated gastric fluid [7,30,31]. Yu et al., explained that ZnO NPs was dissolved only up to 12% and 25% in *ex vivo* and simulated gastric fluid respectively and 5% in serum [21]. Therefore, after oral administration the ZnO NPs were absorbed maximum in the form of NPs matrix and only up to 25% in ionic form and after entering in to the blood it was further dissolved at some extent (up to 15%) and finally internalized in the tissue in ionic as well as NPs form (Table 2). Hence, the present findings support the notion that the oral toxicity of ZnO NPs was stimulated by the contribution of both intact NPs matrix and released Zn^{2+} [32].

The privileged binding property of the b-ZnO NPs was found due to the hydrophobic surface that may interact with a higher affinity with lipid and protein of cell membrane as a result increased the membrane integrity that leads to membrane rupture as compared to c-ZnO NPs (bearing hydrophilic surface). Ramasamy et al., were also found a reduced toxicity of ZnO NPs in human dermal fibroblast cells by surface modification, they explained that the modified hydrophilic surface around capped ZnO NPs were restricting free radical formation, the release of zinc ions, and decreasing surface contact with cells [33]. Due to privileged surface reactive property, b-ZnO NPs might be accelerated higher macrophages associated phagocytosis (MAPs) in liver tissue and also across the hepatocyte membrane as compared to c-ZnO NPs. Toxicity associated with high loading of NPs to mononuclear phagocyte system (MPS) organs are represented by cell stress biomarkers, specifically, subsets of cytokines, chemokines and ROS [34–36]. Furthermore, the NPs internalization into the cells could impel the direct H_2O_2 generation from mitochondria and may produce ROS [37,38]. The ROS generation may increase either due to direct NPs internalization or following the MPS pathway. In our experiment, both treated groups

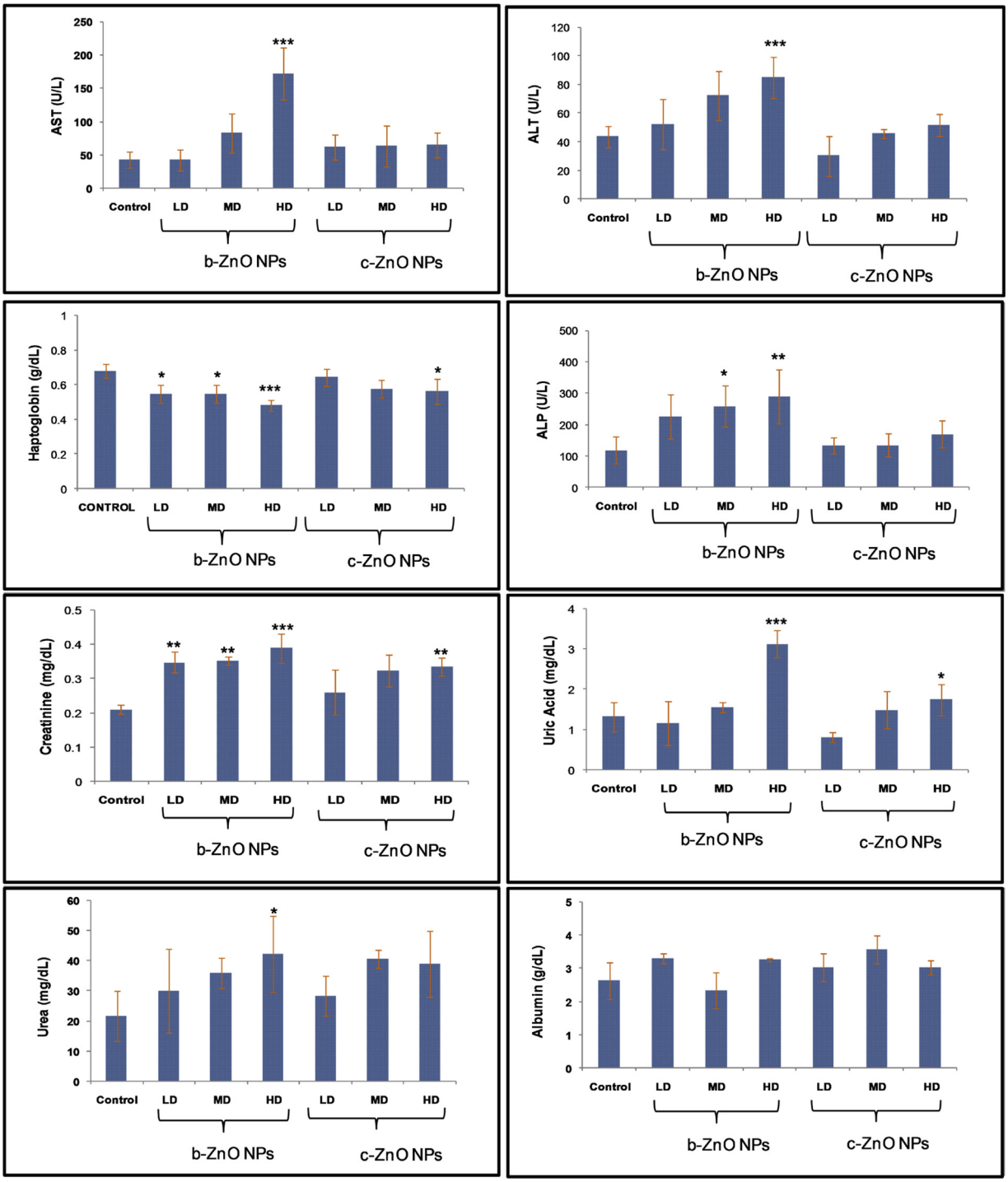

Fig. 10. Alteration in serum hepatotoxic and nephrotoxic biomarkers in Swiss mice after repeated 28 day treatment. Data represented as mean ± SD; n = 10 animals per groups. *, **, *** denotes statistically significant differences at $p < 0.05$, $p < 0.01$, and $p < 0.001$ as compared to control respectively.
NPs- Nanoparticles; c-ZnO NPs-capped Zinc oxide nanoparticles, b-ZnO NPs-bared Zinc oxide nanoparticles, LD- low dose, HD- high dose.

were produced ROS in a similar pattern to the induced hepatic and nephrotoxicity (Fig. 3). The serum creatinine, uric acid, and urea are very potent biomarkers of nephrotoxicity were found increased in the high dose of b-ZnO NPs treated group that was signature of slight necrosis in kidney tissue as seen in histopathology (Fig. 9). The alteration in kidney biomarkers along with pathological lesions was strongly correlated with TEM analysis, The TEM images have revealed damages in kidney tissue in form of ruptured of a large number of mitochondria with total loss of their content, along with lesions in their foot process that were higher in b-ZnO NPs (Fig. 7). These lesions in kidney tissue may affect the glomerular filtration and might be the reason for increased level of serum creatinine, urea and uric acid (Fig. 10). Such type of submicroscopic changes has been also previously reported in the intravenous and subcutaneous treatments [39,40]. Wang et al also reported that urea and creatinine level were increased in mice treated with ZnO NPs at dose of 5 g/kg body weight [7].

The serum LDH, AST, ALP, and ALT are good indicators of hepatic dysfunction and was selected for monitoring liver damages [18,41]. The AST and ALT are abundant in the cytoplasm of hepatocytes, their elevation in serum denotes the altered hepatocellular membrane

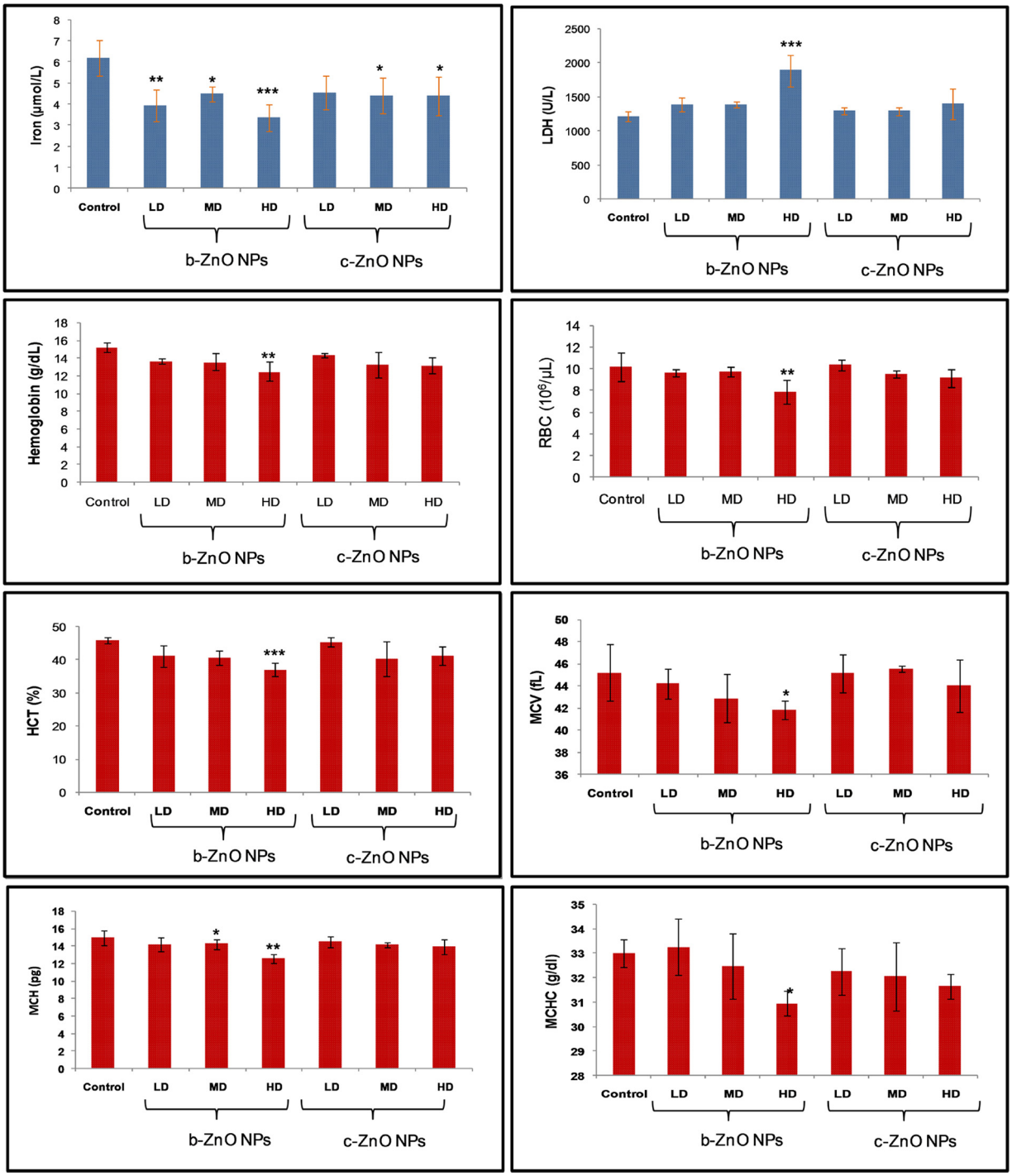

Fig. 11. Hematological parameters change in mice treated with 28 day repeated oral administration. Data represented as mean ± SD; n = 10 animals per groups. *, **, *** denotes statistically significant differences at $p < 0.05$, $p < 0.01$, and $p < 0.001$ as compared to control respectively.
NPs- Nanoparticles; c-ZnO NPs-capped Zinc oxide nanoparticles, b-ZnO NPs-bared Zinc oxide nanoparticles, LD- low dose, HD- high dose.

permeability [42]. After long-term exposure of b-ZnO NPs at the dose of 300 mg/kg, an increasing level of these enzymes was observed in serum which relates to the injury in the hepatocyte cells (Fig. 10). The results were concurrent with histopathological examination of liver tissue, shows a spotty necrosis (Fig. 8). However, TEM images were also depicted diminishes endoplasmic reticulum process, injured mitochondria, higher macrophages and interstitial spaces in cells (Fig. 6). The damages in the liver induced by ZnO NPs, that was revealed by the histopathological examination and serum AST and ALT level [18,30,31]. Similarly, Almansour et al., found liver damage in mice after 21 days repeated oral exposure of ZnO NPs that was revealed by the serum histochemical, ultrastructural and histopathological examination [43]. The liver injury/inflammation clearly enhanced mRNA expression of cytokine (IL-6, MMP-9, and TNF-α), Hp and hepcidin that leads to progression of APR [44–48]. In this study, a significant elevation was found in mRNA expression of hepatic cytokine and proinflammatory biomarkers (IL-6, TNF-α, and MMP-9) in both NPs treated groups at a higher dose but more in b-ZnO NPs, indicating higher APR progression in same (Fig. 12(B)). This result was also consistent with the previous report by Monse et al., who illustrated the dose-dependent

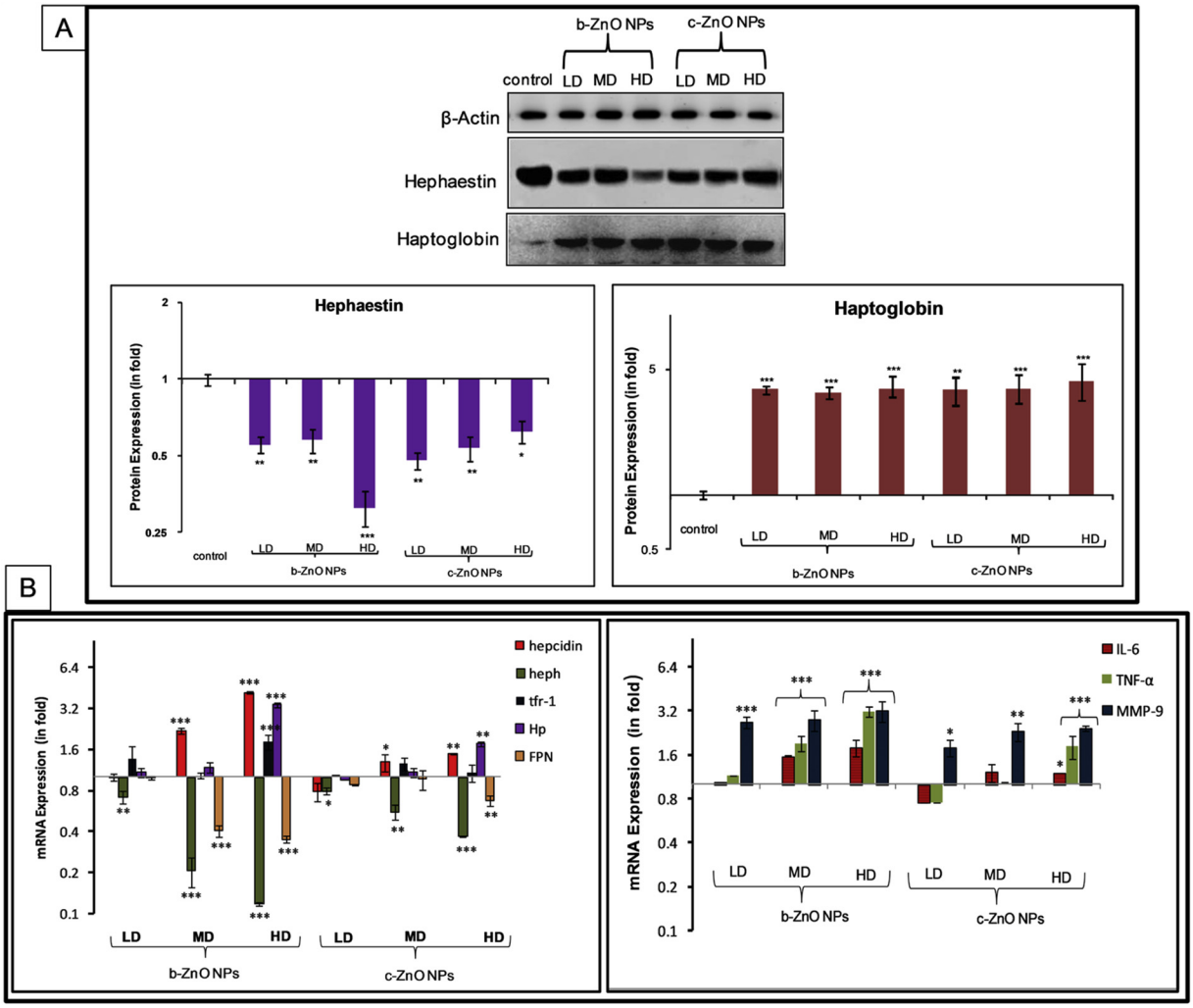

Fig. 12. A: Western blotting for protein expression of Fe signaling protein (haptoglobin and hephaestin) in liver tissue after 28 days repeated oral administration of NPs, The data were normalized with universal biomarkers β-actin. Expression of protein is plotted (in fold *w.r.t* control) on the basis of their band density as analyzed by Image. J.

B: mRNA Expression of Fe signaling gene and pro-inflammatory biomarkers in liver tissue after 28 days repeated oral administration of NPs: the data were represented in fold with respect to control. Data were represented as mean ± SD; n = 5 animals per groups. *, **, *** denotes statistically significant differences at $p < 0.05$, $p < 0.01$, and $p < 0.001$ as compared to control respectively.

NPs- Nanoparticles; c-ZnO NPs-capped Zinc oxide nanoparticles, b-ZnO NPs-bared Zinc oxide nanoparticles, LD- low dose, HD- high dose, TFR-1- transferrin receptor-1, Hp- haptoglobin, heph- hephaestin, FPN-ferroportin.

APR stimulation in humans by inhalation of ZnO nanoparticles [49]. This APR progression could hike the expression of acute phase protein; APPs (Hp and hepcidin) that has a significant role in iron homeostasis [50]. Hepcidin is the main regulator of iron homeostasis in mammals and is up-regulated by pro-inflammatory cytokines [51]. The higher production of liver-derived protein hepcidin during APR, reduces the expression of FPN and hephaestin has been previously reported [52,53]. FPN is cellular iron exporter that controls iron release from duodenal enterocytes and absorb dietary iron from iron-recycling macrophages, and from hepatocytes that store iron [54,55]. Iron release from cells through FPN requires the ferroxidases hephaestin [56]. Binding of hepcidin, triggers FPN internalization, ubiquitination, and subsequent lysosomal degradation that continuing to hold the iron in iron exporting cells, this mechanism is reconciled to hypoferraemia [57]. Accordingly, we found liver hepcidin mRNA expression was up-regulated and this most likely down-regulated the mRNA expression of FPN-1 and Heph in liver and intestine (Figs. 12 and 13). This state might be the reason of low export of Fe in circulation from exporting cells. Additionally, we also observed strong up-regulation of TFR-1 (mRNA) in liver which persuades the uptake of Fe from circulation to hepatic cells. In the previous study an up-regulation of hepatic transferrin, TFR-1 and TFR-2 supported to uptake the circulatory Fe to hepatic cells during the APR [46]. Cumulatively, low absorption of Fe by duodenal enterocyte to circulation and higher uptake from circulation to hepatic cells strongly escorts a condition of hypoferraemia. The c-ZnO NPs induced low ROS and APR relates to low inflammation might be due to their surface modification as compared to b-ZnO NPs, hence c-ZnO NPs slightly altered the Fe signaling pathway. Besides, the administration of excessive Zn through oral route has impaired the absorption of Cu and Fe, hence retardation in growth and anemia were seen [12,58]. Cu is the trace element which is a co-factor for Heph enzyme [53]. In this study, down-regulation of Heph protein expression in liver and intestine was seen that might be the reason for low transportation of Fe into the circulation from liver, duodenal enterocytes, and macrophages (Figs. 12(A) and 13). Resultant, ZnO NPs could alter the Fe signaling pathway by reducing the expression of ferroxidase enzyme Heph, that require for iron exporter protein FPN-1. Wang et al., also concluded that an anemic condition in mice were induced after acute oral treatment of ZnO NPs [7].

The persevered anemic conditions by ZnO NPs were again

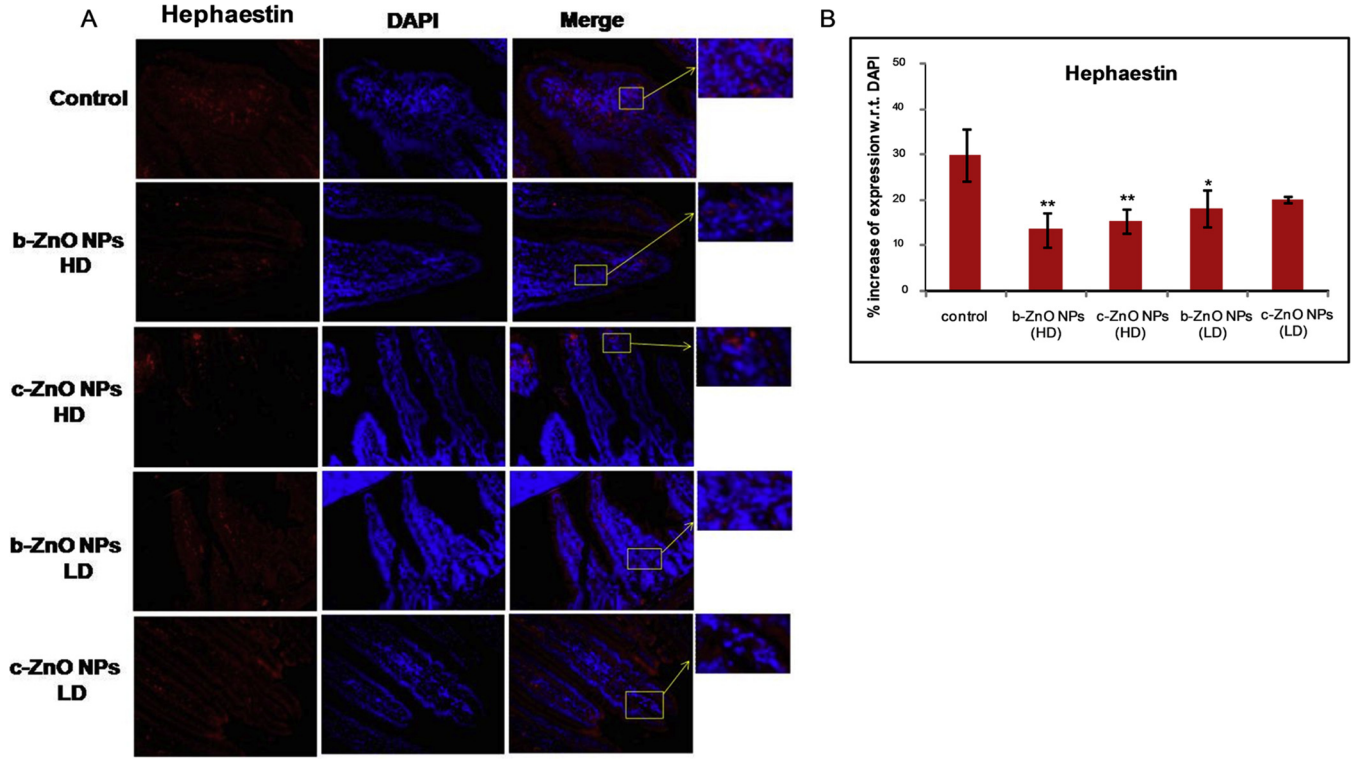

Fig. 13. A: Immunohistochemistry for protein expression of Fe signalling protein (hephaestin) in intestine of female Swiss mice after 28 days repeated oral administration of c-ZnO and b-ZnO NPs at high and low dose only. Immunohistochemistry shows the expression of hephaestin with respect to DAPI (counter stain of nucleus) in b-ZnO NPs (G2), c-ZnO NPs (G4) and control groups. B: The quantitative measurement of expression was performed by RGB analysis on image J software. Bar graphs show means of 5 independent values ± SD. *, **, *** denotes statistically significant differences at $p < 0.05$, $p < 0.01$, and $p < 0.00$ as compared to control respectively.
NPs- Nanoparticles; c-ZnO NPs-capped Zinc oxide nanoparticles, b-ZnO NPs-bared Zinc oxide nanoparticles, LD- low dose, HD- high dose, Heph- hephaestin.

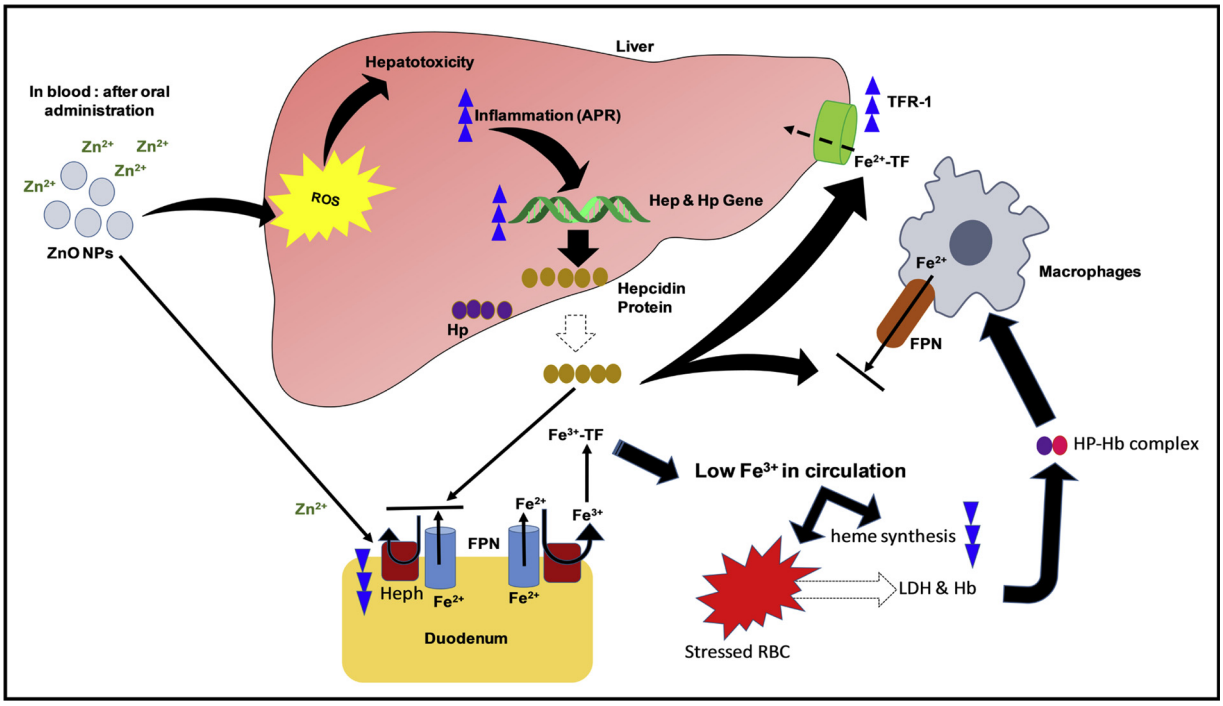

Fig. 14. Graphical Abstract: Role of acute phase responses in alteration of Fe signaling pathways resulting from ZnO NPs treatment. ZnO NPs interact with cell systems and cellular organelles as intact particles as well as ions. Resultant induces inflammation mediated acute phase response that altered the iron homeostasis and promotes anemic condition.
ZnO NPs – Zinc oxide nanoparticles, ROS-reactive oxygen species, APR- Acute phase response, Hep- hepcidin, Hp- haptoglobin, Heph- Hephaestin, FPN- ferroportin, TF- Transferrin receptor, TFR-1- Transferrin receptor-1, LDH- lactate dehydrogenase, Hb-hemoglobin, RBC- red blood cells.

confirmed through a hematological evaluation as found the decreased level of RBC, Hb, HCT, and serum Hp in NPs treated group at high dose (300 mg/kg body weight) (Fig. 11). Rajak et al., has reported that the activity of heme biosynthesis was probably affected by the NPs, would be the main reason for the decreased level of these hematological parameters [59]. The erythropoiesis was affected by Fe homeostasis, Fe deficiency in the body limits the synthesis of heme (a prosthetic group of hemoglobin) that in turn to limit the synthesis of hemoglobin, as a result, decreases the production of RBCs in the bone marrow [60]. In the present study, the decreased lifespan of RBC in circulation might be accelerated due to the deficiency of Fe that indicated the progression of erythropoiesis (suicidal death of RBCs) (Fig. 11) [60]. Furthermore, the increased level of serum LDH is the sign of hemolysis, the LDH diffuse out from the RBC's into the serum at the time of hemolytic condition [61]. Interestingly, the finding of decreased RBC along with increased level of serum LDH was indicated the progression of hemolytic anemia might be driven due to long-term exposure of ZnO NPs at the dose of 300 mg/kg (Fig. 11). This finding correlates with the previous study that defined the size-dependent hemolytic anemia of ZnO NPs in erythrocyte cells [62]. Further Hp analysis in serum and liver were also performed for the confirmation of progression of hemolysis and APR. The serum Hp (APP) is used as one of the biomarkers for the diagnosis of hemolytic anemia and their level increase at the time of inflammation or liver injury [63,64]. It was found that Hp was highly expressed in liver tissue at the higher dose of b-ZnO NPs (Fig. 12), but at the same time, it decreased in serum (Fig. 10). The higher expression of Hp (mRNA and protein) in liver tissues is indicated the APR induction that might be due to the long-term exposure of b-ZnO NPs. These Hp proteins after come into serum might be bind with free hemoglobin (Hb) that was leak out from damaged RBC and formed Hp-Hb complex. The formed Hp-Hb complex may rapidly be cleared through monocyte-macrophage system resultant serum level of Hp was declined. Hence, our findings suggested that 28 days repeated exposure of b-ZnO-NPs at the dose of 300 mg/kg body weight might be impeled APR mediated inflammatory anemia as well as a hemolytic condition which was efficaciously reduced through capping of PAm-g-GG on c-ZnO NPs as summarized in Fig. 14.

5. Conclusion

After oral exposure, ZnO NPs has entered into the circulation and accumulated in secondary target organ in the form of solute and NPs where they were interacted with biological molecules and induced severe toxicity, the surface modification of PAm-g-GG was used as a convincing approach to mitigate the toxicity. The effect of bared b-ZnO and capped c-ZnO NPs were comparably examined after 28 days subacute repeated oral exposure, bared NPs promotes submicroscopic damage in liver and kidney causing a mitochondrial rupture, podocyte swelling and alteration of various hematological and biochemical parameters as compared to c-ZnO NPs. Furthermore, injury/inflammation in cells seemed to activate the acute phase response (APR). The enhanced expression of APPs (hepcidin and Hp) might be the reason to alter interlinked signaling pathway (TFR-1, TFR-2, Heph, transferrin) involved in iron homeostasis. Additionally, the higher Zn ion in circulation has mitigated the expression of iron exporter protein as found in the study. Hence, the long-term exposure of b-ZnO NPs could accumulate in the liver in the form of NPs and ion content that could interfere with the iron signaling pathways by inducing APR or by direct interruption of Fe absorption. Interestingly; the adverse effects of ZnO NPs were minimized by PAm-g-GG coating around NPs in c-ZnO, presumably because of fewer surface interactions of NPs with cells, decreased release rate of zinc ion, and modified hydrophilic surface. This novel surface modulation would suggest a simple yet efficient approach for biomedical utilization of ZnO NPs with reduced side effects. These data is beneficial when concerning the fabrication of ZnO NPs for various biomedical applications.

Conflict of interest

The authors declare no conflict of interest for publication of this work.

Acknowledgment

This research work was supported by a grant from Council of Scientific and Industrial Research (CSIR), New Delhi, India for Nano-Material Applications and Impact on Safety, Health and Environment (NanoSHE) project,(grant No. BSC-0112).

References

[1] S.P. Singh, M. Kumari, S.I. Kumari, M.F. Rahman, M. Mahboob, P. Grover, Toxicity assessment of manganese oxide micro and nanoparticles in Wistar rats after 28 days of repeated oral exposure, J. Appl. Toxicol. 33 (10) (2013) 1165–1179.
[2] J.F. Sargent Jr., Nanotechnology: a Policy Primer, (2013).
[3] A. McWilliams, The maturing nanotechnology market: products and applications, NAN031G, Global Markets, BBC Research Report (2016).
[4] P.K. Stoimenov, R.L. Klinger, G.L. Marchin, K.J. Klabunde, Metal oxide nanoparticles as bactericidal agents, Langmuir 18 (17) (2002) 6679–6686.
[5] T.E. Antoine, Y.K. Mishra, J. Trigilio, V. Tiwari, R. Adelung, D. Shukla, Prophylactic, therapeutic and neutralizing effects of zinc oxide tetrapod structures against herpes simplex virus type-2 infection, Antiviral Res. 96 (3) (2012) 363–375.
[6] J.W. Rasmussen, E. Martinez, P. Louka, D.G. Wingett, Zinc oxide nanoparticles for selective destruction of tumor cells and potential for drug delivery applications, Expert Opin. Drug Deliv. 7 (9) (2010) 1063–1077.
[7] B. Wang, W. Feng, M. Wang, T. Wang, Y. Gu, M. Zhu, H. Ouyang, J. Shi, F. Zhang, Y. Zhao, Acute toxicological impact of nano-and submicro-scaled zinc oxide powder on healthy adult mice, J. Nanoparticle Res. 10 (2) (2008) 263–276.
[8] Jn.F. Hillyer, R.M. Albrecht, Gastrointestinal persorption and tissue distribution of differently sized colloidal gold nanoparticles, J. Pharm. Sci. 90 (12) (2001) 1927–1936.
[9] Y.-N. Chang, M. Zhang, L. Xia, J. Zhang, G. Xing, The toxic effects and mechanisms of CuO and ZnO nanoparticles, Materials 5 (12) (2012) 2850–2871.
[10] Y. Zheng, R. Li, Y. Wang, In vitro and in vivo biocompatibility studies of ZnO nanoparticles, Int. J. Mod. Phys. B 23 (06n07) (2009) 1566–1571.
[11] J. Wang, G. Zhou, C. Chen, H. Yu, T. Wang, Y. Ma, G. Jia, Y. Gao, B. Li, J. Sun, Acute toxicity and biodistribution of different sized titanium dioxide particles in mice after oral administration, Toxicol. Lett. 168 (2) (2007) 176–185.
[12] M.S. Willis, S.A. Monaghan, M.L. Miller, R.W. McKenna, W.D. Perkins, B.S. Levinson, V. Bhushan, S.H. Kroft, Zinc-induced copper deficiency: a report of three cases initially recognized on bone marrow examination, Am. J. Clin. Pathol. 123 (1) (2005) 125–131.
[13] H. Nam, C.-Y. Wang, L. Zhang, W. Zhang, S. Hojyo, T. Fukada, M.D. Knutson, ZIP14 and DMT1 in the liver, pancreas, and heart are differentially regulated by iron deficiency and overload: implications for tissue iron uptake in iron-related disorders, Haematologica 98 (7) (2013) 1049–1057.
[14] J.M. Llobet, J.L. Domingo, M.T. Colomina, E. Mayayo, J. Corbella, Subchronic oral toxicity of zinc in rats, Bull. Environ. Contam. Toxicol. 41 (1) (1988) 36–43.
[15] N.P. Clancey, M.C. Murphy, Zinc-induced hemolytic anemia in a dog caused by ingestion of a game-playing die, Can. Vet. J. 53 (4) (2012) 383.
[16] O. Manuel, P. Fernando, R. Manuel, Inhibition of Iron absorption by zinc: effect of physiological and pharmacological doses: TL015, Pediatr. Res. 60 (5) (2006) 636.
[17] G. Sen, S. Mishra, U. Jha, S. Pal, Microwave initiated synthesis of polyacrylamide grafted guar gum (GG-g-PAM)â€"characterizations and application as matrix for controlled release of 5-amino salicylic acid, Int. J. Biol. Macromol. 47 (2) (2010) 164–170.
[18] A.K. Srivastav, M. Kumar, N.G. Ansari, A.K. Jain, J. Shankar, N. Arjaria, P. Jagdale, D. Singh, A comprehensive toxicity study of zinc oxide nanoparticles versus their bulk in Wistar rats: toxicity study of zinc oxide nanoparticles, Hum. Exp. Toxicol. 35 (12) (2016) 1286–1304.
[19] U.D.N. Bajpai, S. Rai, Grafting of acrylamide onto guar gum using KMnO4/oxalic acid redox system, J. Appl. Polym. Sci. 35 (5) (1988) 1169–1182.
[20] N. Dhiman, A. Singh, N.K. Verma, N. Ajaria, S. Patnaik, Statistical optimization and artificial neural network modeling for acridine orange dye degradation using in-situ synthesized polymer capped ZnO nanoparticles, J. Colloid Interface Sci. 493 (2016) 295–306.
[21] J. Yu, H.-J. Kim, M.-R. Go, S.-H. Bae, S.-J. Choi, ZnO interactions with biomatrices: effect of particle size on ZnO-protein corona, Nanomaterials 7 (11) (2017) 377.
[22] J.-A. Lee, M.-K. Kim, H.-M. Kim, J.K. Lee, J. Jeong, Y.-R. Kim, J.-M. Oh, S.-J. Choi, The fate of calcium carbonate nanoparticles administered by oral route: absorption and their interaction with biological matrices, Int. J. Nanomedicine 10 (2017) 2273.
[23] R. Tiwari, R.D. Singh, H. Khan, S. Gangopadhyay, S. Mittal, V. Singh, N. Arjaria, J. Shankar, S.K. Roy, D. Singh, Oral subchronic exposure to silver nanoparticles causes renal damage through apoptotic impairment and necrotic cell death, Nanotoxicology 11 (5) (2017) 671–686.
[24] X. Jiang, T. MiclÄfuÅŸ, L. Wang, R. Foldbjerg, D.S. Sutherland, H. Autrup, C. Chen, C. Beer, Fast intracellular dissolution and persistent cellular uptake of silver

nanoparticles in CHO-K1 cells: implication for cytotoxicity, Nanotoxicology 9 (2) (2015) 181–189.
[25] K.J. Livak, T.D. Schmittgen, Analysis of relative gene expression data using real-time quantitative PCR and the 2(-Delta Delta C(T)) method, Methods 25 (4) (2001) 402–408.
[26] E.I. Hamilton, M.J. Minski, Abundance of the chemical elements in man's diet and possible relations with environmental factors, Sci. Total Environ. 1 (4) (1973) 375–394.
[27] O. World Health, Trace Elements in Human Nutrition and Health, World Health Organization, 1996.
[28] G. Thennarasu, A. Sivasamy, Synthesis and characterization of nanolayered ZnO/ZnCr2O4 metal oxide composites and its photocatalytic activity under visible light irradiation, J. Chem. Technol. Biotechnol. 90 (3) (2015) 514–524.
[29] C.M. Donangelo, L.R. Woodhouse, S.M. King, F.E. Viteri, J.C. King, Supplemental zinc lowers measures of iron status in young women with low iron reserves, J. Nutr. 132 (7) (2002) 1860–1864.
[30] D. Li-Jing, K. Xiang, J.-H. Liu, Z.-M. Song, Y. Liu, A. Cao, H. Wang, Intestinal injury alters tissue distribution and toxicity of ZnO nanoparticles in mice, Toxicol. Lett. (2018).
[31] H.-J. Paek, Y.-J. Lee, H.-E. Chung, N.-H. Yoo, J.-A. Lee, M.-K. Kim, J.K. Lee, J. Jeong, S.-J. Choi, Modulation of the pharmacokinetics of zinc oxide nanoparticles and their fates in vivo, Nanoscale 5 (23) (2013) 11416–11427.
[32] W. Zhang, Y. Zhao, F. Li, L. Li, Y. Feng, L. Min, D. Ma, S. Yu, J. Liu, H. Zhang, Zinc oxide nanoparticle caused plasma metabolomic perturbations correlate with hepatic steatosis, Front. Pharmacol. 9 (2018) 57.
[33] M. Ramasamy, M. Das, S.S.A. An, D.K. Yi, Role of surface modification in zinc oxide nanoparticles and its toxicity assessment toward human dermal fibroblast cells, Int. J. Nanomedicine 9 (2014) 3707.
[34] B. Fubini, A. Hubbard, Reactive oxygen species (ROS) and reactive nitrogen species (RNS) generation by silica in inflammation and fibrosis, Free Radic. Biol. Med. 34 (12) (2003) 1507–1516.
[35] B. Rimal, A.K. Greenberg, W.N. Rom, Basic pathogenetic mechanisms in silicosis: current understanding, Curr. Opin. Pulm. Med. 11 (2) (2005) 169–173.
[36] N. Fujimura, Pathology and pathophysiology of pneumoconiosis, Curr. Opin. Pulm. Med. 6 (2) (2000) 140–144.
[37] L. Yan, Z. Gu, Y. Zhao, Chemical mechanisms of the toxicological properties of nanomaterials: generation of intracellular reactive oxygen species, Chemistryâ€“An Asian Journal 8 (10) (2013) 2342–2353.
[38] J. Ahmad, M. Ahamed, M.J. Akhtar, S.A. Alrokayan, M.A. Siddiqui, J. Musarrat, A.A. Al-Khedhairy, Apoptosis induction by silica nanoparticles mediated through reactive oxygen species in human liver cell line HepG2, Toxicol. Appl. Pharmacol. 259 (2) (2012) 160–168.
[39] M.A. Ansari, H.M. Khan, A.A. Khan, M.A. Alzohairy, Biochemical and histopathological ultrastructural changes caused by ZnO nanoparticles in mice, Toxicol. Environ. Chem. 97 (8) (2015) 1025–1040.
[40] M. Vivarelli, L. Massella, B. Ruggiero, F. Emma, Minimal change disease, Clin. J. Am. Soc. Nephrol. 12 (2) (2017) 332–345.
[41] D.E. Johnston, Special considerations in interpreting liver function tests, Am. Fam. Physician 59 (1999) 2223–2232.
[42] A. Singh, T.K. Bhat, O.P. Sharma, Clinical biochemistry of hepatotoxicity, J. Clin. Toxicol. S4 (2011) 001, https://doi.org/10.4172/2161-0495.S4-001 J Clinic Toxicol Clinical Pharmacology: Research & Trials ISSN: 2161-0495 JCT, an open access journal, vitro Systems.
[43] M.I. Almansour, M.A. Alferah, Z.A. Shraideh, B.M. Jarrar, Zinc oxide nanoparticles hepatotoxicity: histological and histochemical study, Environ. Toxicol. Pharmacol. 51 (2017) 124–130.
[44] T. Uchida, T. Igarashi, T. Suzuki, K. Kokubun, S. Matsuda, S. Kariyone, The effect of acute inflammation on iron metabolism in rats, Tohoku J. Exp. Med. 139 (3) (1983) 293–298.
[45] E. Nemeth, S. Rivera, V. Gabayan, C. Keller, S. Taudorf, B.K. Pedersen, T. Ganz, IL-6 mediates hypoferremia of inflammation by inducing the synthesis of the iron regulatory hormone hepcidin, J. Clin. Invest. 113 (9) (2004) 1271–1276.
[46] N. Naz, I.A. Malik, N. Sheikh, S. Ahmad, S. Khan, M. Blaschke, F. Schultze, G. Ramadori, Ferroportin-1 is a â€˜nuclearâ€™-negative acute-phase protein in rat liver: a comparison with other iron-transport proteins, Lab. Investig. 92 (6) (2012) 842.
[47] A. Grzanka, E. Machura, M. Misiolek, R. Polaniak, J. Kasperski, A. Kasperska-Zajac, Systemic inflammatory response and calcification markers in patients with long lasting moderate-severe chronic spontaneous urticaria, Eur. J. Dermatol. 25 (1) (2015) 26–28.
[48] M. Czarnecka-Operacz, J. SzulczyÅ„ska-Gabor, K. LeÅ›niewska, E. Teresiak-MikoÅ‚ajczak, P. Bartkiewicz, D. Jenerowicz, K. Wiktorowicz, Z. Adamski, Acute-phase response and its biomarkers in acute and chronic urticaria, Adv. Dermatol. Allergol./PostÈ©py Dermatologii i Alergologii 35 (4) (2018) 400.
[49] C. MonsÃ©, O. Hagemeyer, M. Raulf, B. Jettkant, V. van Kampen, B. Kendzia, V. Gering, Gn. Kappert, T. Weiss, N. Ulrich, Concentration-dependent systemic response after inhalation of nano-sized zinc oxide particles in human volunteers, Part. Fibre Toxicol. 15 (1) (2018) 8.
[50] D. ReczyÅ„ska, M. Zalewska, M. Czopowicz, Ja. Kaba, L. Zwierzchowski, E. Bagnicka, Acute phase protein levels as an auxiliary tool in diagnosing viral diseases in ruminantsâ€”a review, Viruses 10 (9) (2018) 502.
[51] A. Gomes, A. Moreira, Ga. Mesquita, M. Gomes, Modulation of Iron metabolism in response to infection: twists for all tastes, Pharmaceuticals 11 (3) (2018) 84.
[52] T. Ganz, Systemic iron homeostasis, Physiol. Rev. 93 (4) (2013) 1721–1741.
[53] H. Chen, G. Huang, T. Su, H. Gao, Z.K. Attieh, A.T. McKie, G.J. Anderson, C.D. Vulpe, Decreased hephaestin activity in the intestine of copper-deficient mice causes systemic iron deficiency, J. Nutr. 136 (5) (2006) 1236–1241.
[54] D.M. Ward, J. Kaplan, Ferroportin-mediated iron transport: expression and regulation, Biochimica et Biophysica Acta (BBA)-Mol. Cell Res. 1823 (9) (2012) 1426–1433.
[55] M. Enculescu, C. Metzendorf, R. Sparla, M. Hahnel, J. Bode, M.U. Muckenthaler, S. Legewie, Modelling systemic iron regulation during dietary iron overload and acute inflammation: role of hepcidin-independent mechanisms, PLoS Comput. Biol. 13 (1) (2017) e1005322.
[56] C.D. Vulpe, Y.-M. Kuo, T.L. Murphy, L. Cowley, C. Askwith, N. Libina, J. Gitschier, G.J. Anderson, Hephaestin, a ceruloplasmin homologue implicated in intestinal iron transport, is defective in the sla mouse, Nat. Genet. 21 (2) (1999) 195.
[57] M. Nairz, S. Dichtl, A. Schroll, D. Haschka, P. Tymoszuk, I. Theurl, Gn. Weiss, Iron and innate antimicrobial immunityâ€”Depriving the pathogen, defending the host, J. Trace Elem. Med. Biol. (2018).
[58] N.J.N. de Brito, Ãr.D. Rocha, A. de AraÃºjo Silva, Jo.B.S. Costa, M.C. FranÃ§a, M. das GraÃ§as Almeida, J. BrandÃ£o-Neto, Oral zinc supplementation decreases the serum iron concentration in healthy schoolchildren: a pilot study, Nutrients 6 (9) (2014) 3460–3473.
[59] S. Rajak, K. Jamil, Acute and subacute toxicity studies of manganese oxide nanomaterials as compared to bulk in rats with emphasis on changes in biochemical and hematological parameters, Int. J. Adv. Sci. Technol. Res. 2 (2012) 81–94.
[60] E. Nagababu, S. Gulyani, C.J. Earley, R.G. Cutler, M.P. Mattson, J.M. Rifkind, Iron-deficiency anaemia enhances red blood cell oxidative stress, Free Radic. Res. 42 (9) (2008) 824–829.
[61] D.S. Kempe, P.A. Lang, C. Duranton, A. Akel, K.S. Lang, S.M. Huber, T. Wieder, F. Lang, Enhanced programmed cell death of iron-deficient erythrocytes, FASEB J. 20 (2) (2006) 368–370.
[62] E.P. Babu, A. Subastri, A. Suyavaran, K. Premkumar, V. Sujatha, B. Aristatile, G.M. Alshammari, V. Dharuman, C. Thirunavukkarasu, Size dependent uptake and hemolytic effect of zinc oxide nanoparticles on erythrocytes and biomedical potential of ZnO-Ferulic acid conjugates, Sci. Rep. 7 (1) (2017) 4203.
[63] S. Gupta, K. Ahern, F. Nakhl, F. Forte, Clinical usefulness of haptoglobin levels to evaluate hemolysis in recently transfused patients, Adv. Hematol. 2011 (2011).
[64] I.K. Quaye, Haptoglobin, inflammation and disease, Trans. R. Soc. Trop. Med. Hyg. 102 (8) (2008) 735–742.